Original Article

MOLECULAR METABOLISM

A subpopulation of *Bdnf*–e1–expressing glutamatergic neurons in the lateral hypothalamus critical for thermogenesis control

He You [1,2,3], **Pengcheng Chu** [1,2], **Wei Guo** [1], **Bai Lu** [1,*]

ABSTRACT

Objective: Brown adipose tissue (BAT)–mediated thermogenesis plays a key role in energy homeostasis and the maintenance of body temperature. Previous work suggests that brain-derived neurotrophic factor (BDNF) is involved in BAT thermogenesis, but the underlying neural circuits and molecular mechanism remain largely unknown. This is in part due to the difficulties in manipulating BDNF expression in different brain regions through different promoters and the lack of tools to identify neurons in the brain specifically involved in BAT thermogenesis.

Methods: We have created several lines of mutant mice in which BDNF transcription from a specific promoter was selectively disrupted by replacing *Bdnf* with green fluorescent protein (GFP; *Bdnf*-e1, -e4, and -e6$^{-/-}$ mice). As such, cells expressing *Bdnf*-e1, -e4, or -e6 were labeled with GFP. To identify BAT-connected thermogenesis neurons in brain, we applied the retrograde pseudorabies virus labeling method from BAT. We also used chemogenetic tools to manipulate specific neurons coupled with BAT temperature recording. Moreover, we developed a new TrkB agonist antibody to rescue the BAT thermogenesis deficits.

Results: We show that selective disruption of *Bdnf* expression from promoter 1 (*Bdnf*-e1) resulted in severe obesity and deficits of BAT-mediated thermogenesis. Body temperature response to cold was impaired in *Bdnf*-e1$^{-/-}$ mice. BAT expression of *Ucp1* and *Pcg1a*, genes known to regulate thermogenesis, was also reduced, accompanying a decrease in the sympathetic activity of BAT. Staining of cells expressing *Bdnf*-e1 transcript, combined with transsynaptic, retrograde-tracing labeling of BAT-connected neurons, identified a group of excitatory neurons in lateral hypothalamus (LH) critical for thermogenesis regulation. Moreover, an adaptive thermogenesis defect in *Bdnf*-e1$^{-/-}$ mice was rescued by injecting an agonistic antibody for TrkB, the BDNF receptor, into LH. Remarkably, activation of the excitatory neurons (VGLUT2+) in LH through chemogenetic tools resulted in a rise of BAT temperature.

Conclusions: These results reveal a specific role of BDNF promoter I in thermogenesis regulation and define a small subset of neurons in LH that contribute to such regulation.

Keywords Thermogenesis; Brain-derived neurotrophic factor; Lateral hypothalamus; Brown adipose tissue

1. INTRODUCTION

In homothermal animals, such as rodents and human beings, a substantial portion of energy is spent on maintaining body temperature via thermogenesis [1]. In rodents, at the condition of common housing temperature (20–24 °C), about 30%–50% of total energy expenditure comes from cold-induced thermogenesis [2], mainly mediated by brown adipose tissue (BAT) situated in the upper thorax [1]. BAT thermogenesis is controlled by the sympathetic drive, which is connected polysynaptically with neurons in the hypothalamus [3–6]. Because of sympathetic innervation, norepinephrine (NE) release in BAT leads to an increased expression of uncoupling protein 1 (UCP1) [5], a mitochondrial proton carrier in brown adipocytes that uncouples the respiratory chain from adenosine triphosphate (ATP) synthesis, thereby allowing heat generation [5,7].

Brain-derived neurotrophic factor (BDNF) has long been known to play a key role in energy homeostasis, particularly in food intake. Genetic and pharmacological manipulations of BDNF and its receptor TrkB in animals and humans result in obesity, largely due to hyperphagia [8–11]. However, relatively few studies have addressed the role of BDNF in energy expenditure [12–14]. Brain administration of BDNF was found to enhance the release of NE and increase the expression of UCP1 in BAT [13]. Further, infusion of BDNF into the paraventricular hypothalamus (PVH) increases energy expenditure coupled with elevation of UCP1-mediated thermogenesis [15]. In contrast, only energy expenditure, but not UCP1 levels in BAT, were increased when BDNF was injected into the ventral medial hypothalamus (VMH) [14]. These results suggest that exogenously applied BDNF could regulate BAT thermogenesis through brain control of the sympathetic nervous system.

[1]School of Pharmaceutical Sciences, Tsinghua University, Beijing, 100084, China [2]School of Life Sciences, Tsinghua University, Beijing, 100084, China [3]Tsinghua-Peking Center for Life Sciences, Tsinghua University, Beijing, 100084, China

*Corresponding author. E-mail: bai_lu@tsinghua.edu.cn (B. Lu).

Received October 23, 2019 • Revision received November 16, 2019 • Accepted November 17, 2019 • Available online 22 November 2019

https://doi.org/10.1016/j.molmet.2019.11.013

Although pharmacologic studies have revealed a role of BDNF in thermogenesis, the underlying mechanisms remain largely unknown. A major reason lies in the distribution of BDNF in many different brain regions, which contributes to a plethora of brain functions by promoting synaptic transmission and plasticity [16–21]. It is difficult to establish the specific brain regions, neural circuits, and cell types that mediate BDNF regulation of thermogenesis. One feasible approach is to knockout the *Bdnf* gene in different hypothalamic subregions specifically. Indeed, genetic deletion of *Bdnf* in PVH resulted in hyperphagia and reduced energy expenditure, suggesting that PVH BDNF is also involved in thermogenesis [12]. However, it is challenging to tease apart how BDNF differentially regulates thermogenesis and food intake in PVH [6]. Moreover, such region-specific knockout approaches could not discover new regions/circuits, resulting in less robust effects.

To overcome the above limitations and discover new brain regions and mechanisms contributing to BDNF regulation of thermogenesis, we have taken a different approach: to examine thermogenesis in animals with genetic mutations on different *Bdnf* promoters, which drive BDNF expression in a subset of brain regions. The genomic structure of *Bdnf* is quite unique. There are 9 upstream promoters; each drives a small exon that is alternatively spliced onto a common exon 10, which encodes the entire BDNF protein [22]. Thus, there are 9 different *Bdnf* transcripts in the brain coding for the same BDNF protein [23]; each may be expressed in specific types of neurons in distinct brain areas and developmental stages and/or regulated differentially by environmental factors. Using knock-in mouse lines in which an individual promoter was specifically disrupted, we have shown that different *Bdnf* transcripts can be linked to different signaling pathways and behaviors [24–28].

In the present study, we hypothesized that different *Bdnf* promoters may mediate different aspects of energy homeostasis. Indeed, disruption of *Bdnf* promoter I (*Bdnf*-e1$^{-/-}$), but not promoter IV (*Bdnf*-e4$^{-/-}$) or VI (*Bdnf*-e6$^{-/-}$), expression resulted in severe deficits in thermogenesis. With green fluorescent protein (GFP) labeling driven by *Bdnf* promoter I, we identified discrete neuronal populations in the brain expressing *Bdnf*-e1 transcript. The thermogenesis-related neuronal circuits were labeled using a transsynaptic, retrograde-tracing technique. By combining the two techniques, we have identified a subset of neurons in the lateral hypothalamus (LH) that were both thermogenesis related and *Bdnf*-e1 deficient. Activation of the BDNF receptor TrkB in these neurons by injecting a TrkB agonistic antibody to LH rescued some of the thermogenesis deficits in *Bdnf*-e1$^{-/-}$ mice. Remarkably, we found that those *Bdnf*-e1+/BAT–connected neurons are glutamatergic, and activating excitatory neurons (VGULT2+) in LH through chemogenetic tools leads to a rise of BAT temperature. These results define a new role of promoter I–derived BDNF and identified a unique group of LH *Bdnf*-e1–expressing neurons critical for thermogenesis.

2. METHODS

2.1. Animals

Bdnf-e1$^{-/-}$, -e4$^{-/-}$, and e6$^{-/-}$ mice were generated as previously described [26] (see Table S1 for primers for genotyping), in which transcription from promoter I, IV, or VI produced eGFP protein instead of BDNF protein. Vgat-IRES-Cre (Stock No.028862) and Vglut2-IRES-Cre (Stock No. 028863) mice were from Jackson Laboratory. The animals were kept on a 12 h:12 h light/dark cycle with ad libitum access to water and a regular rodent chow (No. 1032 or No. 1035, 12-mm irradiated pelleted, consisting of (proximate analysis) 10% moisture, 20.0% crude protein, 4.0% crude oil, 5.0% crude fiber, 8.0% ash, 1.0–1.8% calcium, and 0.6–1.2% phosphorus (Huafukang Biology co., Beijing, China). All experiments were conducted in accordance with a protocol (AP# 16-LB2) approved by the Tsinghua University Animal Care and Use Committee.

2.2. Cold exposure and temperature measurement

Mice were translocated to a 4 °C incubator for 1 h, and rectal temperature was measured subsequently every half hour with a standard thermo-probe (A579, THERMOMETER, BIOSEB, Vitrolles, France) inserted in to the rectum (2.0-cm depth). BAT temperature was measured after 2 days by an IPTT-300 micro-thermosensor implanted subcutaneously above BAT.

2.3. Molecular biology studies

2.3.1. Tissue preparations

Age-matched adult male mice (wild type [WT] and *Bdnf*-e1$^{-/-}$) were euthanized by CO_2. Liver, BAT, gonadal white adipose tissue (WAT), medium prefrontal cortex (mPFC), amygdala, cerebellum, hypothalamus, and hippocampus were dissected and collected on ice. For micro-dissection of LH, dorsal medial hypothalamus (DMH), and VMH, ~1-mm-thick coronal brain slices (Bregma −0.94 mm, −1.94 mm) were immediately prepared from fresh brain tissue by a Brain Matrices (RWD Life Science Co., Ltd., Product No. 68707). LH, DMH, and VMH were then dissected under 10× bright-field microscopy with ophthalmic scissors and forceps. These tissues were immediately used for the following processes or frozen at −80 °C for later use.

2.3.2. RNA extraction

Total RNA was isolated and extracted from targeted tissues using TRIzol (Invitrogen) according to the manufacturer's instructions. RNA was subsequently treated with DNase I (Takara) to remove genome DNA and quantified using a NanoDrop spectrophotomer (Denovix, Wilmington, USA). For quantitative polymerase chain reaction (qPCR), RNA was reverse transcribed into cDNA using PrimerScript™ RT Master Mix (TaKaRa) following the manufacturer's protocol.

2.3.3. qPCR

Quantitative PCR was performed with a CFX96 Touch™ Real-Time PCR Detection System (BIO-RAD) using SYBR® Premix Ex Taq™ II (Takara, Code No. RR820A) following the recommended two-step protocol. Primers used for qPCR were commercially synthesized (Life Technologies). *Actb* was used as a reference gene. See Table S2.

2.3.4. Protein extraction

Dissected hypothalamus and hippocampus from each mouse were homogenized by grinding in 1 mL of ice-cold RIPA lysis buffer, followed by centrifugation for 30 min at 17,000×*g* at 4 °C. Supernatants were then collected, and 200-μl aliquots were used to assess the total protein concentration using the BCA Protein Assay Kit [29]. For western blotting, total protein concentrations were added with loading buffer and heated to 95 °C for 10 min.

2.3.5. Western blotting

Total protein concentrations with loading buffer were fractionated via electrophoresis using a 10% sodium dodecyl sulfate–polyacrylamide gel electrophoresis gel (BIO-RAD) and transferred onto activated polyvinylidene difluoride membranes (BIO-RAD). Membranes were incubated in blocking buffer (5% bovine serum albumin in 0.1 M tris buffered saline with Tween) for 1 h at room temperature and then in primary antibody dilution buffer overnight at 4 °C. After sufficient

washing, membranes were incubated in secondary antibody (1:2500) dilution buffer. Again, after sufficient washing, signal detection (Tanon 5200, Shanghai, China) was achieved with SuperSignal™ West Pico Chemiluminescent Substrate (Thermo Scientific). The protein bands were analyzed using ImageJ image analysis software. The primary antibodies used for immunoblotting were anti-TH (rabbit, 1:500, CST), TrkB (rabbit, 1:1000, CST), pTrkB (rabbit, 1:1000, CST), AKT (rabbit, 1:1000, Easybio), pAKT (rabbit, 1:1000, CST), PLCγ (rabbit, 1:1000, CST), pPLCγ (rabbit, 1:1000, CST), ERK (rabbit, 1:1000, CST), pERK (rabbit, 1:1000, CST), GAPDH (mouse, 1:5000, Easybio), and anti-β-tubulin (rabbit, 1:2500, Easybio).

2.3.6. BDNF ELISA

BDNF protein levels were determined by a two-sided enzyme-linked immunosorbent assay (ELISA; R&D SYSTEMS) as described by the manufacturer. Lysates were loaded directly into 96-well plates without dilution. Absorbance was recorded and analyzed using a Cytation BioTeK plate reader (Winooski, USA). BDNF concentration (pg/ml) was normalized to total soluble protein (mg/ml) in each sample, and data were expressed as percentage change of WT (pg BDNF/mg total protein).

2.4. NE content measurement in BAT by the liquid chromatography-mass spectrometry method

BAT was dissected immediately after deep anesthetization with Avertin (500 mg/kg) and transferred to a 1.5-ml Eppendorf tube. Prechilled high-performance liquid chromatography—grade methanol (at −80 °C) was added to the tube according to the weight of the BAT tissue, with 100 μl per 10 mg of tissue. Tissues were homogenized for 1 min with tissue grinder on dry ice, vortexed for 30 s at 4 °C, and incubated at −80 °C for 2 h. After centrifugation at 14,000×*g* for 20 min at 4 °C, 500 μl supernatant was transferred to a new 1.5-ml Eppendorf tube. The supernatant was further lyophilized to pellet with Speedvac (Thermo Savant SPD1010). The dried samples were used for the NE measurement or stored in a −80 °C freezer. The Dionex Ultimate 3000 ultra-performance liquid chromatography system was coupled to a TSQ Quantiva Ultra triple-quadrupole mass spectrometer (Thermo Fisher, CA), equipped with a heated electrospray ionization probe in positive ion mode. For NE analysis, a BEH amide column (1.7 μm, 2.1 × 50 mm, Waters) was used. Mobile phase A was prepared by 95% acetonitrile and 5% water with 10 mM ammonium formate. pH was adjusted to 3.0 with formate solution. Mobile phase B was prepared by mixing 50% water with 10 mM ammonium formate and 50% acetonitrile and subsequently adjusting pH to 3.0 with formate solution. The linear gradient was 0 min, 2% B; 1.2 min, 2% B; 4.5 min, 98% B; 6 min, 98% B; 6.1 min, 2% B; and 8 min, 2% B. The flow rate was 0.25 ml/min. The column chamber and sample tray were held at 35 °C and 10 °C, respectively. Data were acquired in selected reaction monitoring for NE with transition of 170/107. Precursor and fragment ion were collected with a resolution of 0.7 full width at half maximum, respectively. The source parameters were as follows: spray voltage, 3500 V; ion transfer tube temperature, 350 °C; vaporizer temperature, 300 °C; sheath gas flow rate, 30 Arb; auxiliary gas flow rate, 10 Arb; and CID gas, 1.5 mTorr. To calculate the absolute value of BAT NE content, a linear standard curve was drawn by measuring 4, 8, 80, 400, and 2000 ng NE standard samples. Data analysis and quantitation were performed by the software Xcalibur 3.0.63 (Thermo Fisher, CA).

2.5. PRV inoculation

Recombinant pseudorabies virus (PRV) inoculation was performed in a biosafety level-2 operating room, according to a previous study [30]. Mice were anesthetized with Avertin (200 mg/kg) and then were settled in a brain stereotaxic apparatus (RWD Life Science Co., Shenzhen, China). After the interscapular BAT was exposed, three 500-nl injections of a PRV (PRV-614, 10^9 pfu/ml, BrainVTA, Wuhan, China) were made into the brown fat on one side using a 10-ul Hamilton syringe with a 31-gauge needle. Shortly after surgery, mice received metacam (1 mg/kg) for analgesia and were translocated to their home cages. At the 6th day after microinjection, the animals were deeply anesthetized by Avertin (350 mg/kg) and perfused with phosphate-buffered saline (PBS; 0.1 M) and paraformaldehyde (PFA; 4%).

2.6. Immunohistochemistry

Mice were deeply anaesthetized with Avertin (350 mg/kg) and transcardially perfused with PBS and 4% PFA sequentially. Brains were postfixed overnight, cryoprotected in 30% sucrose, and cut with a frozen microtome in coronal 50-μm sections. Brain sections were translocated into 24-well plates filled with 1 ml blocking buffer (5% goat serum, 0.3% Triton™ X-100 [Triton was not added when staining membrane proteins, such as TrkB] in 0.1M PBS) for 1 h in the orbital shaker (80 r/min). The 24-well plates were incubated at 4 °C in the orbital shaker (60 r/min) after adding primary antibody. Brain slices in the plate were washed by PBS three times and incubated with secondary antibody at 4 °C overnight. Brain slices were incubated in Hoechst (5 μg/ml) for 10 min at room temperature, washed by PBS three times, and then mounted in mounting medium (H-1400, Vector Laboratories, Inc.) for confocal imaging (Zeiss LSM780 confocal microscope). Primary antibodies for immunostaining were GFP (chicken, 1:100, AVES), TrkB (mouse, 1:50, Santa Cruz), mRFP (rabbit, 1:1000, Takara), orexin (mouse, 1:200, Santa Cruz), MCH (mouse, 1:200, Santa Cruz), and cFos (rabbit, 1:1000, Synaptic Systems).

2.7. Primary mouse cultures of hypothalamic neurons

Pregnant mice at embryonic day 16—17 (E16-E17) were euthanized after being anesthetized with high-dose Avertin (400 mg/kg). Embryonic hypothalamic regions were dissected from brains on ice-cold DPBS immediately as a previous protocol described [31]. Hypothalamic tissues were digested with EDTA Trypsin (0.125%, Gibco) at 37 °C for 15 min. The protease activities of trypsin were neutralized with plating medium (DMEM, 10% fetal bovine serum, 2 mM GlutaMAX™ Supplement, 1 mM sodium pyruvate; Gibco), and the brain tissues were gently triturated 4 to 5 times with a 1-ml pipette. Cells were filtered with a 40-μm Nylon mesh filter and plated with plating medium in a 6-well dish at a density of ∼4 × 10^5 cells per well. The plating medium was removed 4 h later and replaced with 3 ml maintenance medium (Neurobasal medium, 1x B27 supplement, 2 mM GlutaMAX™ supplement, 1 mM sodium pyruvate; Gibco). Half of the maintenance medium was changed every 3 days. At DIV7, hypothalamic neurons were treated with TrkB-agomab or BDNF for western blot analysis.

2.8. Stereotaxic injection of AAV and TrkB agonistic antibody

Mice were anesthetized with Avertin (200 mg/kg) and then settled in a brain stereotaxic apparatus (RWD Life Science Co., Shenzhen, China). For adeno-associated virus (AAV) injection, 100 nl AAV-DIO-hM3Dq-mCherry, or AAV-DIO-mCherry (OBiO Technology [Shanghai] Corp., Ltd., 1012 titer) was administered bilaterally into the LH of *Bdnf*-e1$^{-/-}$ mice using a 10-ml Hamilton syringe with a 33-gauge needle. For antibody injection, 200 nl TrkB-agomab (3.4 mg/ml) or mouse normal IgG (3.4 mg/ml) was administered bilaterally into the LH of *Bdnf*-e1$^{-/-}$ mice using a 10-ml Hamilton syringe with a 33-gauge needle. Infusion of the antibody (200 nl, 20 nl/min) was accomplished by a micro-

syringe pump (KD Scientific, Holliston, USA). The following coordinates defined LH location: anteroposterior, −1.58 mm; mediolateral, ±1.0 mm; and dorsoventral, −4.80 mm relative to the bregma. At the end of the infusion, the needle was left in the brain for another 5 min to reduce backflow of the antibody. Shortly after surgery, mice received metacam (1 mg/kg) for analgesia and were translocated to their home cages.

2.9. Statistical analysis

Statistical analyses were performed using GraphPad Prism Software. The animal sample size for each study was chosen on the basis of literature documentation of similar well-characterized experiments, and no statistical method was used to predetermine sample size. Samples or animals were randomly assigned to experimental groups if applicable. No sample or animal was excluded from the analysis. Unpaired Student's *t*-test was used for comparison between the two genotypes (WT and *Bdnf*-e1$^{-/-}$) *t*, whereas analysis of variance tests were performed for multiple samples comparison, followed by post hoc Bonferroni analysis. All data were expressed as mean ± SEM. Statistical significance was set at $P < 0.05$ as *, $P < 0.01$ as **, and $P < 0.001$ as ***.

3. RESULTS

3.1. Obesity phenotype in *Bdnf*-e1$^{-/-}$ mice

To investigate the role of specific *Bdnf* promoters in energy balance regulation, we used mice in which one of the *Bdnf* promoters was selectively mutated. These mice were generated by inserting an enhanced green fluorescent protein (eGFP) followed by multiple STOP codons (eGFP-STOP cassette) downstream of a noncoding exon, respectively, as previously described (for example, e1 and e4 mutants shown in Figure 1A,B) [27]. Genotyping analysis revealed structural alteration of exon I and exon IV, respectively, in e1$^{-/-}$ and e4$^{-/-}$ mice (Figure S1A–D). The insertion of the eGFP-STOP cassette resulted in transcription of mutant e1 mRNA instead of WT e1 mRNA (Figure S1E–F) and translation of eGFP instead of BDNF protein (Figure S1G).

As an initial step toward characterizing mice with mutation in BDNF promoter I (*Bdnf*-e1$^{-/-}$), which is known to be regulated by neuronal activity [32], we recorded their body weight from 2 months to 9 months of age (Figure 1C). With normal chow feeding, we observed that *Bdnf*-e1$^{-/-}$ mice became overweight starting around 3 months of age, and their body weight reached a plateau (about 50 g) at 6 months of age, compared with their WT littermates, which had a plateau of approximate 30 g (Figure 1C). At 6 months of age, *Bdnf*-e1$^{-/-}$ mice also had a ~8-mm longer body length compared with WT (Figure 1D). Similar to BDNF promoter I, BDNF promoter IV is highly regulated by neuronal activity [32]. We therefore performed the same experiments using the promoter IV mutant mice (*Bdnf*-e4$^{-/-}$). In contrast to the *Bdnf*-e1$^{-/-}$ mice, the body weight of *Bdnf*-e4$^{-/-}$ male mice appeared normal at 2, 3, and 6.5 months of age (Figure 1E), suggesting that *Bdnf* promoter I but not promoter IV participates in energy balance regulation. To confirm that the obesity phenotype occurred only in adulthood, we measured the body weight of *Bdnf*-e1$^{-/-}$ male mice before sexual maturity. From 4 weeks to 8 weeks of age, there was no difference in body weight between WT and *Bdnf*-e1$^{-/-}$ mice (Figure 1F). A similar obesity phenotype was also observed in 4-month-old female mice (Table S3).

The micro–computed tomography technique, which could effectively detect different types of fat tissues based on their densities [33], was used to further examine adipose depots in WT and *Bdnf*-e1$^{-/-}$ mice (Figure 1G,H). We found that both BAT and WAT were enlarged in *Bdnf*-e1$^{-/-}$ mice at 9 months of age. Notably, in WT mice, there was nearly no detectable adipose depot in the pleural cavity, while fat was found to accumulate around the heart and aorta in *Bdnf*-e1$^{-/-}$ mice (Figure 1H). Quantitative analysis of several adipose depots of BAT and WAT (subcutaneous WAT [SWAT], visceral WAT [VWAT], and heart surrounding WAT [HWAT]; Figure 1I and Video 1, 2), with volume normalized to body weight, indicated that enlarged adipose tissues make a major contribution to the overweight phenomenon in *Bdnf*-e1$^{-/-}$ mice.

Supplementary video related to this article can be found at https://doi.org/10.1016/j.molmet.2019.11.013.

3.2. Impaired BAT thermogenesis in *Bdnf*-e1$^{-/-}$ mice

As we observed the enlarged BAT, we next investigated whether the morphology and function of BAT were impaired in *Bdnf*-e1$^{-/-}$ mice. We first examined and compared the cell morphology in the BAT of *Bdnf*-e1 and e4$^{-/-}$ mice. Hematoxylin and eosin staining of BAT paraffin-embedded tissue sections revealed a dramatic change in cellular morphology, with larger lipid droplets in brown adipocyte cells of *Bdnf*-e1$^{-/-}$ mice (Figure 2A). Quantitative analysis of droplet number per square millimeter in BAT sections indicated a significant decrease in droplet number in *Bdnf*-e1$^{-/-}$ mice, suggesting an increase in the lipid droplet size (Figure 2B). However, *Bdnf*-e4$^{-/-}$ mice showed a normal size of lipid droplets in brown adipocyte cells.

We next examined the expression of thermogenesis-related genes in BAT by real-time qPCR (Figure 2C). One of the key thermogenesis genes is *Ucp1*. It is a mitochondrial transmembrane protein that uncouples protons moving down their mitochondrial gradient from ATP synthesis, allowing energy to be dissipated as heat [29]. The expression of *Ucp1* mRNA was dramatically decreased in the BAT of *Bdnf*-e1 but not e4$^{-/-}$ mice. Similarly, the mRNA level of *Pgc1a*, a transcriptional coactivator regulating the expression of genes involved in thermogenesis including *Ucp1*, was also decreased in *Bdnf*-e1$^{-/-}$ BAT.

Previous studies have suggested that adaptive thermogenesis could reflect BAT thermogenesis ability [34]. We next measured adaptive thermogenesis directly by cold exposure experiment. WT and *Bdnf*-e1$^{-/-}$ mice were translocated into a 4 °C incubator for a short period (1 h), during which rectal temperature was measured (Figure 2D). We first observed a mild decrease in the rectal temperature when the *Bdnf*-e1$^{-/-}$ mice were at room temperature (Figure 2D, 0 h), indicating decreased thermogenesis in their baseline state. Next, we found that cold exposure resulted in a much greater decrease in rectal temperature in the *Bdnf*-e1$^{-/-}$ mice compared with that in WT mice, further demonstrating deficiency in adaptive thermogenesis in *Bdnf*-e1$^{-/-}$ BAT (Figure 2D, 1 h). The experiments of cell morphology, gene expression, and thermogenic function together suggest that selective disruption of promoter I–driven BDNF expression results in a significant deficit in BAT-mediated baseline thermogenesis as well as adaptive thermogenesis.

To determine whether *Bdnf*-e1 transcript is expressed in nonneuronal tissues and whether BDNF could function directly in the periphery to regulate BAT thermogenesis, we measured levels of *Bdnf*-e1 transcript and BDNF protein in liver, BAT, and WAT. Unlike in the brain, no *Bdnf*-e1 transcript was detected in liver, BAT, or WAT (Figure S2A). Indeed, we found a very low level of BDNF protein in liver, BAT, or WAT but a moderate level in muscle and heart (Figure S2B). However, no significant difference was observed between WT and *Bdnf*-e1$^{-/-}$ mice in any of those peripheral tissues. These findings suggest that the *Bdnf*-e1 transcript functions mainly in the brain rather than in peripheral

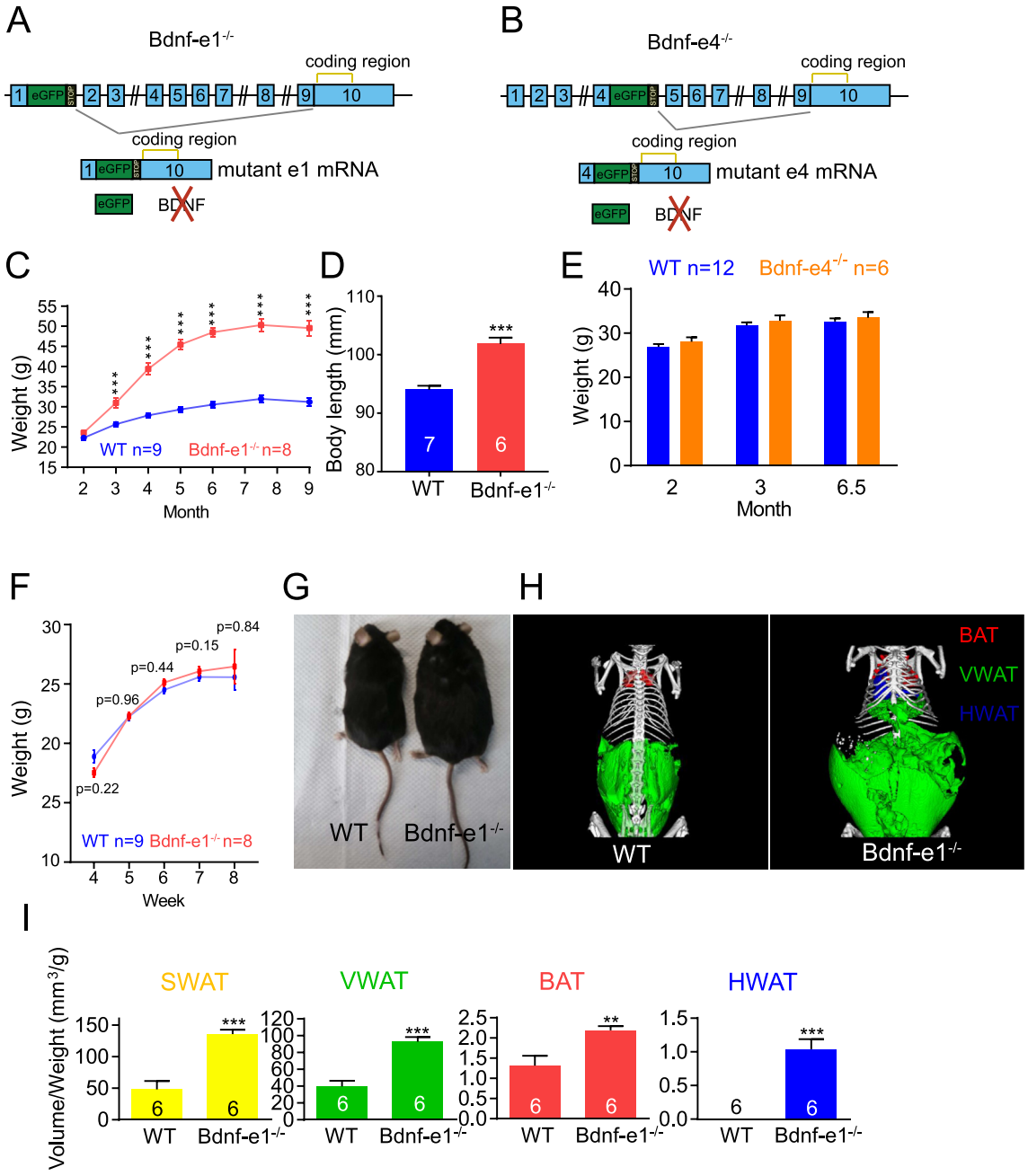

Figure 1: Severe obesity in mice with specific disruption of BDNF expression from promoter I. (A–B) Strategy for generating mice with specific disruption of BDNF expression from exon 1 (a: *Bdnf*-e1) or exon 4 (b: *Bdnf*-e4). The *Bdnf* gene in the mouse has 9 noncoding exons (exon 1–9, blue rectangles) and one coding exon (exon 10, blue rectangle with coding region noted). Each noncoding exon could be transcribed from its respective promoter and alternatively spliced to exon 10 to translate the same BDNF protein. An eGFP-STOP cassette (eGFP, green rectangle, followed by multiple stop codons, black-shaded rectangle) is inserted after exon 1 to generate *Bdnf*-e1 mutant mice. In *Bdnf*-e1$^{-/-}$ mice, the e1 transcript (mutant e1 mRNA) driven by promoter I expresses eGFP but not BDNF protein because of the presence of stop codons. **(C)** Body weight of WT (blue) and *Bdnf*-e1$^{-/-}$ (red) male mice from 2 months to 9 months of age. **(D)** Body length of WT (blue) and *Bdnf*-e1$^{-/-}$ (red) male mice at the age of 6 months. **(E)** Body weight of WT (blue) and *Bdnf*-e4$^{-/-}$ (orange) male mice at 2, 3, and 6.5 months. **(F)** Body weight change before sexual maturity in WT and Bdnf-e1$^{-/-}$ mice. **(G)** Photographs of WT and *Bdnf*-e1$^{-/-}$ mice at 9 months of age. **(H)** Micro–computed tomography images of bone (white), VWAT (green), BAT (red), and HWAT (blue) in WT and *Bdnf*-e1$^{-/-}$ mice with pseudo-color. **(I)** Normalized volume of SWAT, VWAT, BAT, and HWAT with body weight in WT and *Bdnf*-e1$^{-/-}$ mice. In this and all other figures, data are shown as mean ± SEM; n.s., no significant change; *$p < 0.05$; **$p < 0.01$; ***$p < 0.001$. "n" or the number associated with each column represents the number of animals used. Note that a marked body weight increase was observed in *Bdnf*-e1$^{-/-}$ mice as early as 3 months.

tissues for BAT thermogenesis, although this brain-specific transcript is globally knocked out in our *Bdnf*-e1$^{-/-}$ mice.

BAT-mediated thermogenesis is controlled by sympathetic outflow. Activation of β-noradrenergic receptors on brown adipocyte membrane by NE released from sympathetic nerve terminals results in an increase in UCP1 [3,5]. We directly measured the NE level in the BAT of WT and *Bdnf*-e1 and e4$^{-/-}$ mice using liquid chromatography–mass spectrometry (see the Methods section). There

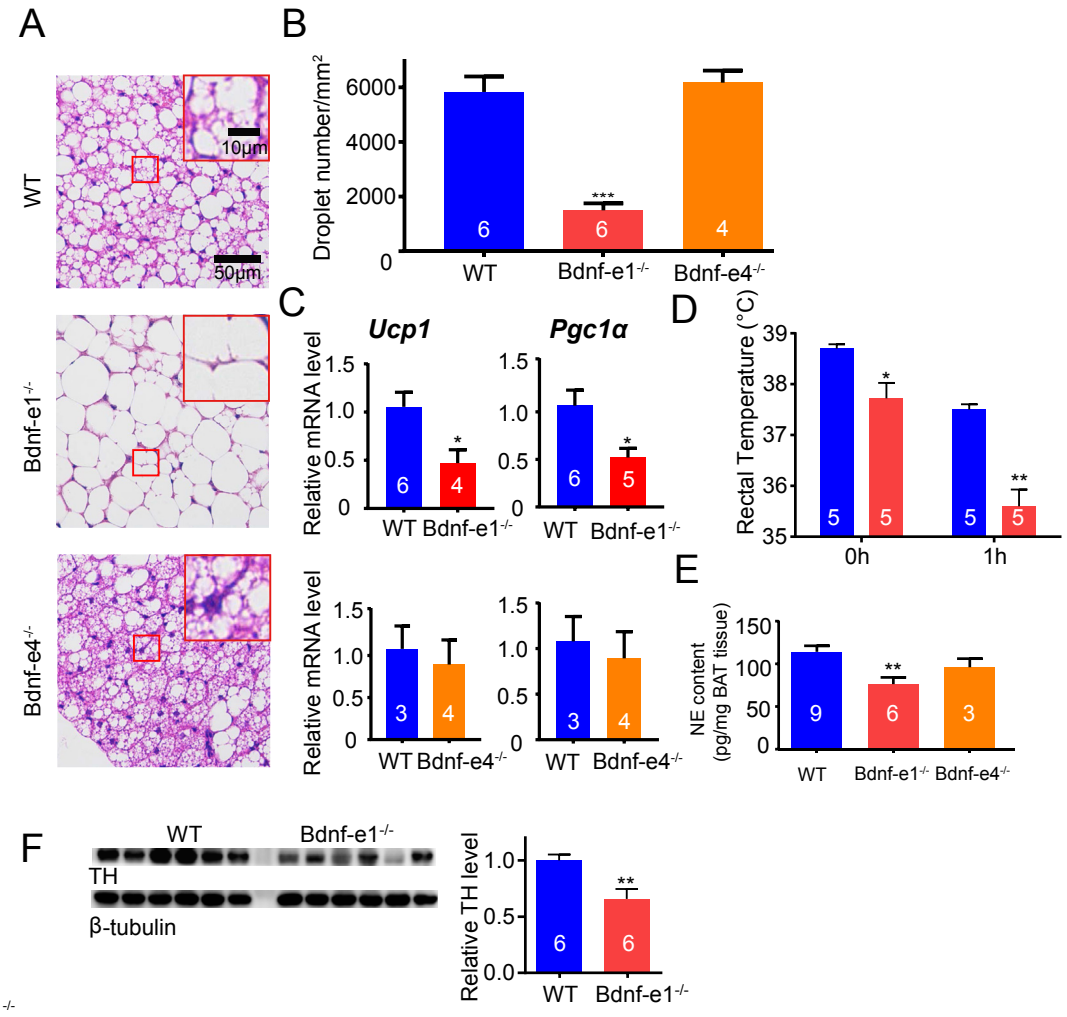

Figure 2: Impairment of BAT-mediated thermogenesis and sympathetic outflow in *Bdnf*-e1$^{-/-}$ mice. (A) Hematoxylin and eosin (HE) staining of BAT in WT, *Bdnf*-e1$^{-/-}$, and *Bdnf*-e4$^{-/-}$ mice at ~5 months of age. Upper right corner, enlarged images of the red rectangular areas. Note that the lipid droplets are much larger in the BAT of *Bdnf*-e1$^{-/-}$ mice as compared with those in WT mice. **(B)** Droplet number per mm^2 in the BAT sections of WT, *Bdnf*-e1$^{-/-}$, and *Bdnf*-e4$^{-/-}$ mice. A smaller average number means larger lipid droplets in the BAT of *Bdnf*-e1$^{-/-}$ mice. Paraffin-embedded BAT sections of those mice were used for HE staining and statistics. **(C)** Expression of thermogenesis-related genes (*Ucp1* and *Pcg1a*) in the BAT of WT, *Bdnf*-e1$^{-/-}$, and *Bdnf*-e4$^{-/-}$ mice at ~5 months of age. Relative levels of *Ucp1* and *Pcg1a* mRNAs in BAT from *Bdnf*-e1$^{-/-}$ mice were normalized to those from WT mice after a real-time qPCR assay. **(D)** Rectal temperature of WT and *Bdnf*-e1$^{-/-}$ mice at room temperature and after exposing animals to 4 °C for 1 h. **(E)** Levels of NE in BAT of WT, *Bdnf*-e1$^{-/-}$, and *Bdnf*-e4$^{-/-}$ mice measured by the LS-MS method. **(F)** Immunoblotting of tyrosine hydrolase (TH), a marker for sympathetic innervation, of BAT extracts from WT and *Bdnf*-e1$^{-/-}$ mice. β-tubulin was used as a loading control. Quantification of the immunoblot shown in a lower panel. The TH levels in BAT from *Bdnf*-e1$^{-/-}$ mice were normalized to those from WT mice.

was a significant decrease in the NE level in *Bdnf*-e1 but not in e4$^{-/-}$ mice, compared with that in WT mice (Figure 2E). In addition, we found that the level of tyrosine hydrolase (TH), the rate-limiting enzyme in NE synthesis and also a marker for sympathetic nerve activity [12], was significantly decreased in the BAT of *Bdnf*-e1$^{-/-}$ mice (Figure 2F). Thus, the deficit in thermogenesis seen in adult *Bdnf*-e1$^{-/-}$ mice could be due to an attenuated sympathetic activity in BAT.

Next, we investigated whether BAT thermogenesis was the cause or consequence of obesity. The BAT analyses above were performed at the age of 10–11 weeks (<3 months), prior to overt obesity observed in *Bdnf*-e1$^{-/-}$ mice. Both the body weight and body length exhibited a trend of increase but showed no statistical significance at this time point (Figure 3A,B). However, the BAT weight (Figure 3C) and Ucp1 mRNA (Figure 3D) expression of *Bdnf*-e1$^{-/-}$ mice were significantly decreased compared with WT mice. Moreover, we found that the TH level was decreased (Figure 3E,F), indicating a reduced sympathetic outflow well before the overt obesity phenotype was observed. Taken together, the deficits of BAT thermogenesis could be one of the contributors that result in the obesity phenotype in *Bdnf*-e1$^{-/-}$ mice.

3.3. Distribution of *Bdnf*-e1 transcript in brain

To establish the link between *Bdnf* promoter I disruption and the deficit in BAT sympathetic outflow, we need to map the distribution of the *Bdnf*-e1 transcript in the brain (Figure 4). The design of our knock-in mice is such that the *Bdnf* exon 1 is followed by an eGFP sequence with multiple stop codons. Western blot reliably detected eGFP expression in the hypothalamus of the *Bdnf*-e1$^{-/-}$ mice (Figure S1B). Immunostaining using an anti-eGFP antibody (see the Methods section) detected the *Bdnf*-e1–driven eGFP, revealing cells with a high level of *Bdnf*-e1 expression. In coronal sections of the *Bdnf*-e1$^{-/-}$ brain, *Bdnf*-e1–expressing neurons were reliably observed in the following five brain regions (Figure 4A–E): cingulate cortex 2 (Cg2),

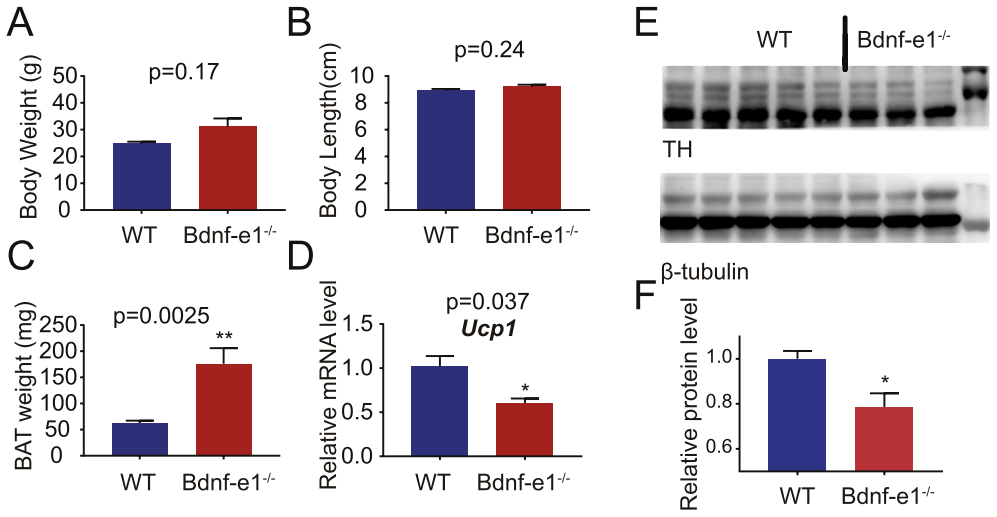

Figure 3: BAT analyses at the age of onset of weight gain. (A–C) Body weight (**A**), body length (**B**), and BAT weight (**C**) of WT and *Bdnf*-e1$^{-/-}$ mice 10–11 weeks old, when the body weight just begins to rise. **(D)** Expression of *Ucp1* mRNAs in BAT. Data from *Bdnf*-e1$^{-/-}$ mice were normalized to those from WT mice after a real-time qPCR assay. **(E)** Immunoblotting of tyrosine hydrolase (TH), a marker for sympathetic activity, of BAT extracts from WT and *Bdnf*-e1$^{-/-}$ mice. β-tubulin was used as a loading control. **(F)** Quantification of the immunoblot in (**e**). The TH levels in BAT from Bdnf-e1−/− mice were normalized to those from WT mice. In this figure, WT mice n = 5; *Bdnf*-e1$^{-/-}$ mice n = 5, 10–11 weeks.

basal lateral amygdala (BLA), LH, medial amygdaloid nucleus (MePV), and amygdalopiriform transition area (APir). In some other regions, such as PVH (Figure 4F), ventromedial hypothalamus (VMH) (Figure S3A), and dentate gyrus (DG) (Figure S3B), we observed fewer neurons with fainter *Bdnf*-e1–driven eGFP signals.

Among the five regions with strong *Bdnf*-e1–eGFP expression, LH was the only one previously implicated in BAT thermogenesis [35]. Therefore, we examined BDNF production in the LH of *Bdnf*-e1$^{-/-}$ mice with BDNF ELISA. BDNF protein in LH, when normalized to total proteins, decreased by approximately 50% in *Bdnf*-e1$^{-/-}$ mice, compared with WT animals (Figure 4G). However, BDNF protein in VMH showed no significant decrease in *Bdnf*-e1$^{-/-}$ mice. Taken together, a disruption of promoter I–driven BDNF expression in LH may contribute to the thermogenesis deficit in *Bdnf*-e1$^{-/-}$ mice.

To determine whether the thermogenesis deficit in *Bdnf*-e1$^{-/-}$ mice was due to the disruption of *Bdnf* promoter I alone, we measured the expression of other *Bdnf* transcripts in different brain regions. As expected, disruption of promoter I did not alter *Bdnf* transcription through promoter II, IV, or VI at 9 months of age in the hypothalamus, mPFC, amygdala, or hippocampus (Figure S4A–E). Notably, the expression of e2 and e6 transcripts in the cerebellum was decreased, and that of e6 transcript in the mPFC was slightly increased. As the cerebellum and mPFC are generally not involved in thermogenesis, the slight changes of other promoters' activities in these two brain regions might not contribute to the impaired BAT thermogenesis in *Bdnf*-e1$^{-/-}$ mice. Finally, we focused on the hypothalamus and examined all remaining transcripts of BDNF (e3, e5, e7, e8, e9). No significant difference was found between the two genotypes in any of these transcripts (Figure S4F). Thus, *Bdnf* promoter I is perhaps the key promoter involved in thermogenesis.

3.4. Distribution of BAT-connected neurons in brain

To identify a key region(s) involved in the thermogenesis, we needed to examine all brain areas directly and indirectly innervating or projecting to BAT. By injecting into BAT the PRV, which is known to undergo multiple, trans-synaptic retrograde transport [36,37], we were able to label the entire neuronal circuits connected to BAT. Six days after infection of PRV-614-mRFP (red fluorescent protein) in BAT, the brain sections were immunostained with antibodies against PRV driven mRFP. Six brain areas were found to be connected to BAT, including S1HL (primary sensory cortex, hindlimb region) (Figure 5A), PVH (Figure 5B), LH (Figure 5C), VMH (Figure 5D), periaqueductal gray (PAG) (Figure 5E), and raphe pallidus nucleus (RPa) (Figure 5F). Among these areas, only LH was found to also express *Bdnf-e1*–eGFP, raising the possibility that *Bdnf-e1* and PRV are co-expressed in the same neurons in LH.

3.5. *Bdnf*-e1–expressing neurons in BAT thermogenesis

To determine whether *Bdnf*-e1–expressing neurons may connect to BAT, we used a double-labeling method. Combining PRV-614-mRFP tracing and *Bdnf-e1*–driven eGFP immunostaining, we investigated which group of *Bdnf*-e1–expressing neurons was involved in neuronal circuits subserving BAT thermogenesis. Six days after infection of PRV-614-mRFP in BAT of *Bdnf*-e1$^{-/-}$ mice, the brain sections were immunostained with antibodies against PRV-driven mRFP and *Bdnf*-e1–driven eGFP. In agreement with previous studies [38] and our data (Figure 5), neurons in several brain regions including two hypothalamic nuclei, PVH (Figure 6A,B) and LH (Figure 6C,D), were labeled by BAT-derived PRV-614-mRFP.

A previous study showed that BDNF in the BAT-connected PVH neurons regulates sympathetic outflow to BAT [12]. However, the retrogradely labeled PVH neurons (red) did not express *Bdnf*-e1–driven eGFP (green) (Figure 6A,B), suggesting that these BAT-connected PVH neurons do not use *Bdnf*-e1–derived BDNF to regulate BAT functions. Interestingly, we found that BAT-connected neurons (red) in LH expressed *Bdnf*-e1–driven eGFP (green) (Figure 6C,D). Quantitative analysis revealed that close to 90% of thermogenesis-related neurons in LH were labeled with *Bdnf*-e1–driven eGFP (Figure 6E). Moreover, we found the *Bdnf*-e1 expression in other regions that could drive BAT, including the preoptic area ventromedial part (VMPO), VMH, and RPa [37]. However, we found no overlap between *Bdnf*-e1–expressing neurons and BAT-connected

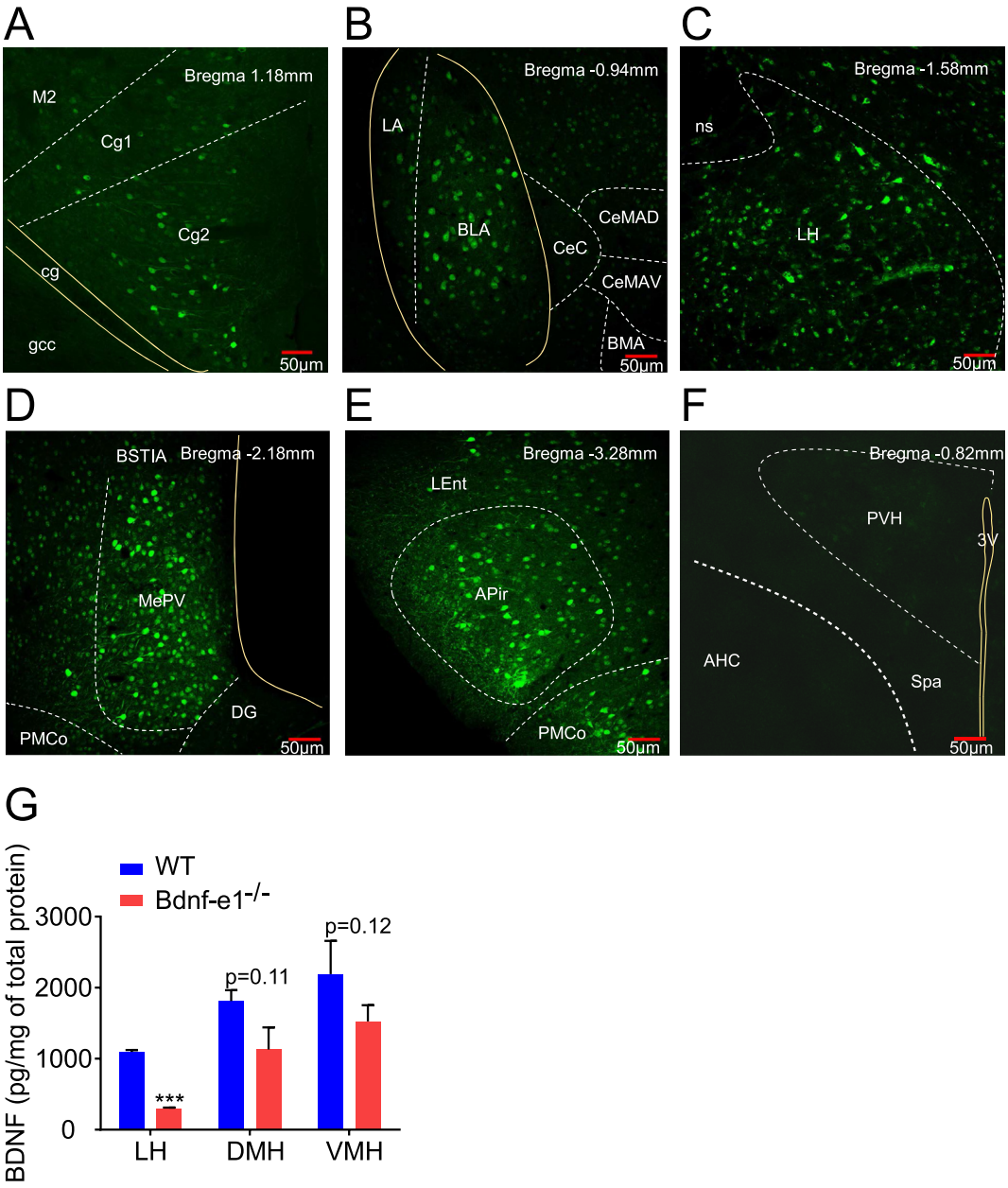

Figure 4: Expression of BDNF in *Bdnf*-e1$^{-/-}$ mouse brain. (A–E) Immunofluorescent staining of *Bdnf*-e1–driven eGFP in cross sections through *Bdnf*-e1$^{-/-}$ mice brain from caudal to rostral. The green fluorescence indicates cells in which *Bdnf*-e1–driven expression of BDNF is disrupted. Dashed lines (white) indicate the separation of nucleus or subnucleus; solid lines (yellow) indicate neuronal fibers or brain ventricles. Scale bar (red), 50 μm. **(A)** Bregma 1.18 mm eGFP fluorescence was detected in Cg2 (cingulate cortex, area 2). Cg1, cingulate cortex, area 1; M2, secondary motor cortex; gcc, genu of the corpus callosum; cg, cingulum. **(B)** Bregma −0.94 mm eGFP fluorescence was expressed selectively in BLA (basal lateral amygdala) and LA (lateral amygdala) but not CeC (central amygdaloid nucleus, capsular part), CeMAD (central amygdaloid, medial division, anterodorsal part), CeMAV (central amygdaloid, medial division, anteroventral part), or BMA (basomedial amygdaloid nucleus). Note a fairly confined expression of eGFP in BLA. **(C)** Bregma −1.58 mm. In the hypothalamus, eGFP fluorescence was largely confined to the LH. ns, nigrostriatal bundle. **(D)** Bregma −2.18 mm eGFP fluorescence was expressed selectively in the MePV (medial amygdaloid nucleus). BSTIA, bed nucleus of the stria terminalis, intra-amygdaloid division; PMCo, posteromedial cortical amygdaloid nucleus; DG, dentate gyrus; cp, cerebral peduncle. **(E)** Bregma −3.28 mm eGFP fluorescence was expressed in APir (amygdalopiriform transition area) and the part of caudal PMCo. LEnt, lateral entorhinal cortex. **(F)** Bregma −0.82 mm eGFP fluorescence was hardly detected in PVH. AHC, anterior hypothalamic area, central part. SPa, subparaventricular zone of the hypothalamus. 3V, the third ventricle. **(G)** Expression of BDNF protein in LH, DMH, and VMH of WT and *Bdnf*-e1$^{-/-}$ mice. BDNF protein levels were normalized with total lysed protein. A two-site BDNF ELISA was used to quantify the level of BDNF protein.

neurons in the VMPO (Figure S5A) or DMH/VMH (Figure S5B), and no *Bdnf*-e1 expression was detected in the RPa (Figure S5C). Taken together, we have identified a new population of *Bdnf*-e1–expressing BAT-connected neurons in LH that are potentially involved in thermogenesis.

3.6. Attenuation of thermogenesis defect by restoring BDNF-TrkB signaling in LH

To investigate the function of promoter I–derived BDNF in BAT-connected LH neurons, we examined the expression of TrkB, the receptor of BDNF in these neurons. As shown in Figure 7A, many

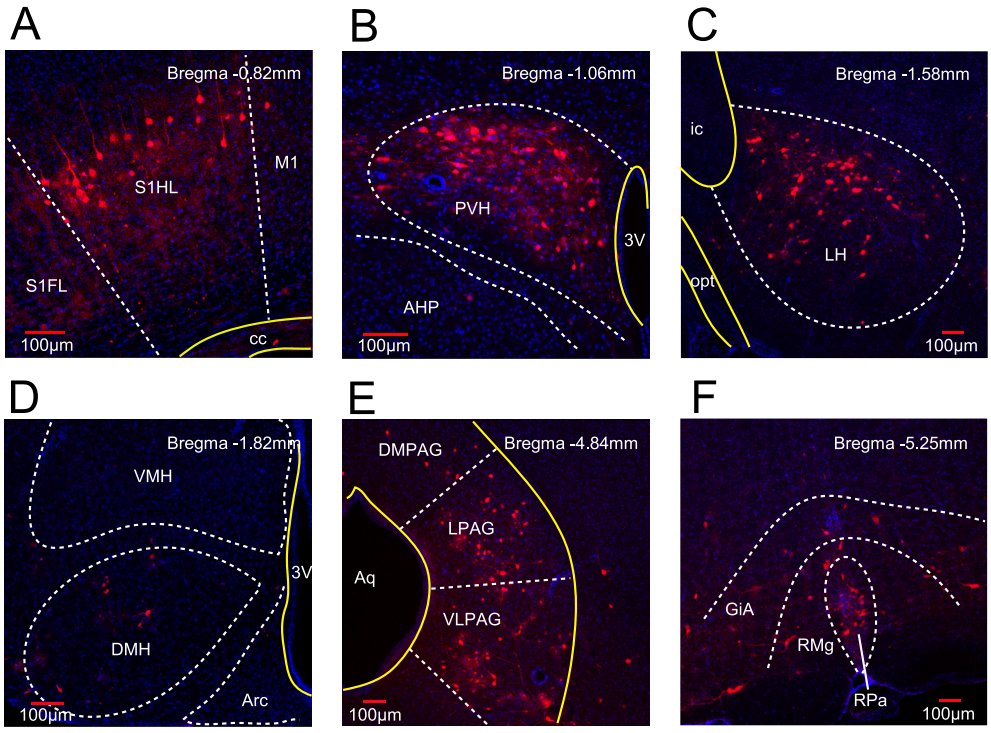

Figure 5: BAT-connected neurons in mouse brain. (A–F) Immunostaining images showing BAT-connected neurons in six brain areas. PRV-614-mRFP, a transsynaptic retrograde tracer labeling neuronal circuits, was injected into the left BAT of mice. These mice were processed for immunostaining 6 days after PRV infection. Dashed lines (white) indicate the separation of the nucleus or subnucleus; solid lines (yellow) indicate neuronal fibers or brain ventricles. Scale bar (red), 100 μm. **(A)** Bregma −0.82 mm. PRV mRFP fluorescence was detected in S1HL (primary sensory cortex, hindlimb region). S1FL, primary sensory cortex, forelimb region; M1, primary motor cortex; cc, corpus callosum. **(B)** Bregma −1.06 mm. PRV fluorescence was expressed in the PVH (paraventricular hypothalamus). AHP, anterior hypothalamic area, posterior part; 3V, the third ventricle. **(C)** Bregma −1.58 mm. PRV fluorescence was expressed in LH. opt, optic tract; ic, internal capsule. **(D)** Bregma −1.82 mm. A few PRV + neurons were detected in the VMH. DMH, dorsal medial hypothalamus; Arc, arcuate hypothalamic nucleus. **(E)** Bregma −4.84 mm eGFP fluorescence was expressed in the PAG (periaqueductal gray), mainly including the lateral part (LPAG) and dorsolateral part (DLPAG). A few PRV + neurons were detected in the DMPAG (dorsomedial part PAG). Aq, aqueduct. **(F)** Bregma −5.25 mm. PRV fluorescence was expressed in RPa (raphe pallidus nucleus), RMg (raphe magnus nucleus), and GiA (gigantocellular reticular nucleus, alpha part).

neurons in LH were immunoreactive for TrkB. Interestingly, double staining of TrkB and PRV-driven mRFP revealed that virtually all BAT-connected neurons expressed TrkB (Figure 7B,C). To ensure the specificity of TrkB staining, we used a different TrkB antibody. Again, we found that most BAT-connected neurons were TrkB immunoreactive (data not shown).

If a reduction of *Bdnf*-e1—derived BDNF in LH leads to the BAT thermogenic deficit, activation of BDNF-TrkB signaling locally in LH neurons should alter at least some aspects of BAT thermogenesis. BDNF is a sticky protein with a very short half-life [21,39]. We therefore used a specific TrkB agonist, a monoclonal antibody named TrkB-agomab [40], for the rescue experiment. In primary cultured hypothalamic neurons, application of TrkB-agomab for 1 h elicited a robust, dose-dependent phosphorylation of TrkB tyrosine kinase and triggered its three main downstream signaling pathways, PLC-γ, AKT, and MAPK (Figure 7D). We then examined whether infusion of TrkB-agomab locally to LH could attenuate thermogenesis deficits in *Bdnf*-e1$^{-/-}$ mice. The TrkB-agomab was delivered bilaterally into LH (Figure 7E,

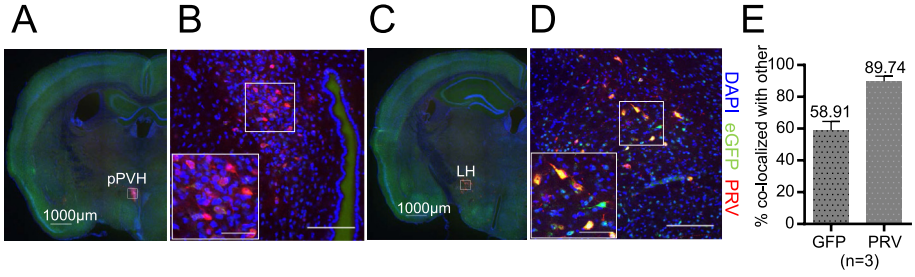

Figure 6: Expression of *Bdnf*-e1 in BAT-connected neurons in LH. (A–D) Immunostaining images showing the co-expression of *Bdnf*-e1—driven eGFP (green) and PRV-614-mRFP (red) in LH (**C-D**) but not in PVH (**A-B**). PRV-614-mRFP was injected into the left BAT of *Bdnf*-e1$^{-/-}$ mice at 3 months of age. These mice were processed for immunostaining 6 days after injection. Coronal sections of frozen brain were used for double-staining of eGFP and mRFP. (**B**) and (**D**) are the enlarged confocal immunostaining images (scale bar, 50 μm) in the white rectangular areas of (**A**) and (**C**), respectively. **(E)** Percentage of *Bdnf*-e1—eGFP neurons positive for PRV infection (left), and percentage of PRV-positive neurons stained for *Bdnf*-e1—driven eGFP (right) in the LH. Note that ~90% of thermogenesis-related neurons express *Bdnf*-e1 transcript.

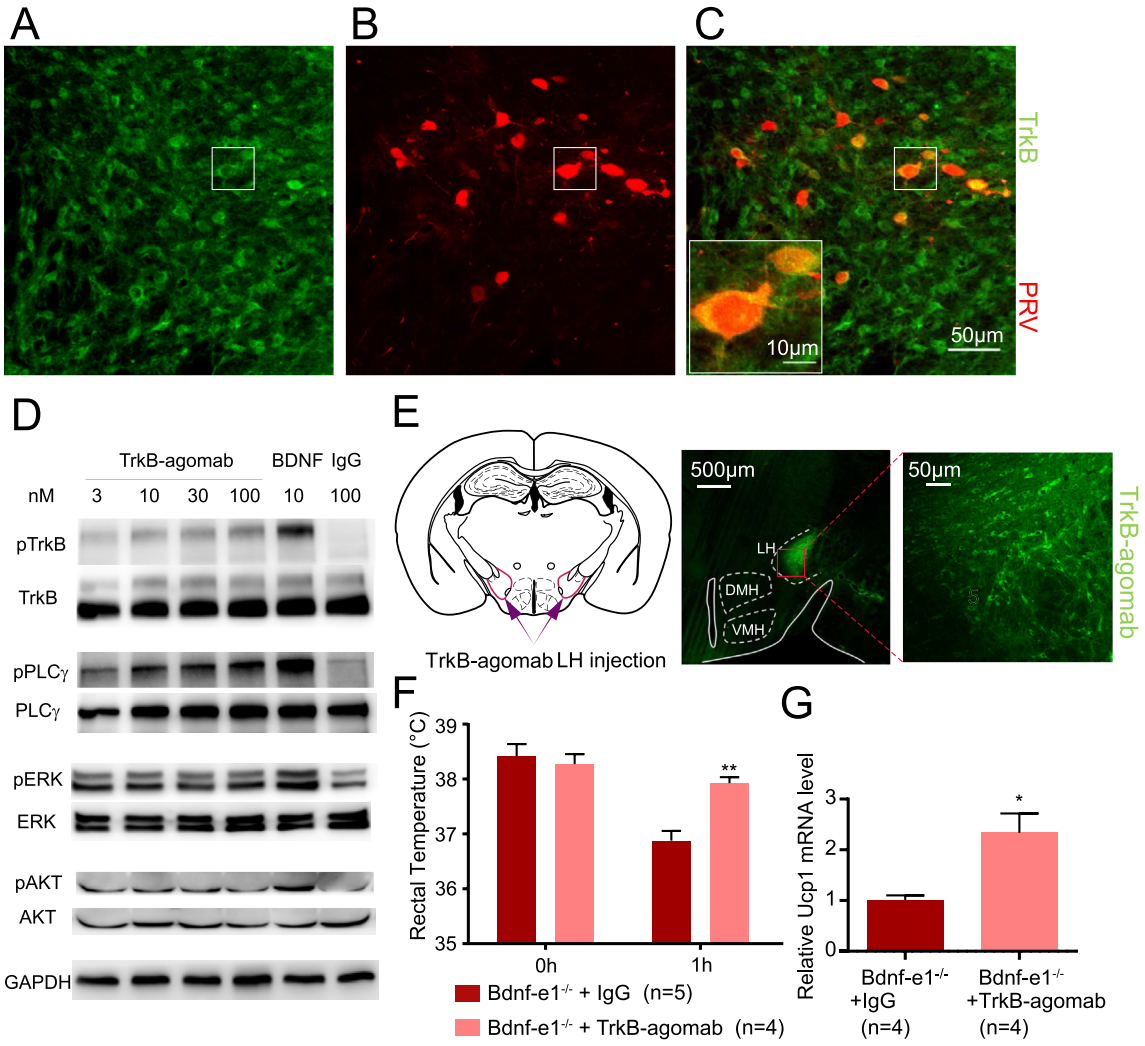

Figure 7: Rescue of thermogenesis deficit by injecting TrkB agonistic antibody into LH. (A–C) Immunostaining of TrkB (green) and PRV-614-mRFP (red) in LH. Note the punctate staining of TrkB on BAT-connected PRV-mRFP^{+} neurons. **(D)** Western blot showing BDNF-TrkB signaling activated by the TrkB agonistic antibody TrkB-agomab in DIV7 cultured hypothalamic neurons. **(E)** Schematic diagram (left) and staining photos (right) showing that TrkB-agomab was bilaterally injected into LH. The injection site was marked with purple lines in the coronal section (left), and the enlarged image of the injection site stained with anti-mouse IgG is shown on the right. **(F)** Effect of TrkB agonistic antibody on rectal temperature. *Bdnf*-e1$^{-/-}$ mice (4 months old) received bilateral injections of either IgG or TrkB agonistic antibody into LH and recovered for 3 days. Rectal temperatures were measured at room temperature and 1 h after the animals were exposed to 4 °C. **(G)** Effect of TrkB agonistic antibody (TrkB-agomab) on the expression of thermogenesis marker *Ucp1* in BAT. *Bdnf*-e1$^{-/-}$ mice (4 months old) received a bilateral injection of either IgG or TrkB agonistic antibody into the LH and were housed in their home cages for 2 weeks. *Ucp1* mRNA expression in BAT was measured by real-time qPCR. The data for the TrkB-agomab–treated group were normalized to the IgG-treated group.

left; 200 nl, 3.4 ng/ul), and 3 days after injection, substantial amounts of the mouse TrkB-agomab were detected in LH using a goat anti-mouse-IgG antibody (Figure 7E, right). Rectal temperature was monitored in a cold exposure experiment [41]. After 1 h of exposure to 4 °C, the *Bdnf*-e1$^{-/-}$ mice injected with a control antibody (IgG, 200 nl, 3.4 ng/ul) to bilateral LH showed a marked decrease in rectal temperature (Figure 7F). In contrast, in the *Bdnf*-e1$^{-/-}$ mice injected with the same amount of TrkB-agomab, the decreased rectal temperature during cold exposure was markedly attenuated (Figure 7F). Moreover, the thermogenesis marker *Ucp1* expression in BAT was also increased 2 weeks after TrkB-agomab injection (Figure 7G). It is conceivable that there are also TrkB-expressing afferent fibers in LH. Thus, activation of TrkB on *Bdnf*-e1 neurons or TrkB-expressing fibers in LH could rescue the deficit in adaptive thermogenesis in *Bdnf*-e1$^{-/-}$ mice.

3.7. *Bdnf-e1*+/BAT-connected neurons are glutamatergic and their contribution to BAT thermogenesis

We further determined the nature of these LH *Bdnf-e1*+/BAT-connected neurons. First, an AAV-DIO-mCherry virus was injected in the LH of Vgat or Vglut2-IRES-cre mice to label specifically the GABAergic or glutamatergic neurons in LH. Next, another PRV (PRV-152-GFP) was injected into the BAT of these mice to label retrogradely all thermogenesis-related neurons. Because there was about 90% overlap between the *Bdnf*-e1–expressing and the BAT-connected neurons, the PRV-152-GFP–positive cells essentially represent the newly identified "thermogenesis related" neurons in LH. Surprisingly, most BAT-connected LH neurons (PRV-GFP^{+}, green) expressed mCherry signal (red) in Vglut2 (Figure 8A) but not Vgat-cre mice (Figure 8B). A preliminary characterization showed that within the subregion where the BAT-connected neurons were located, there was

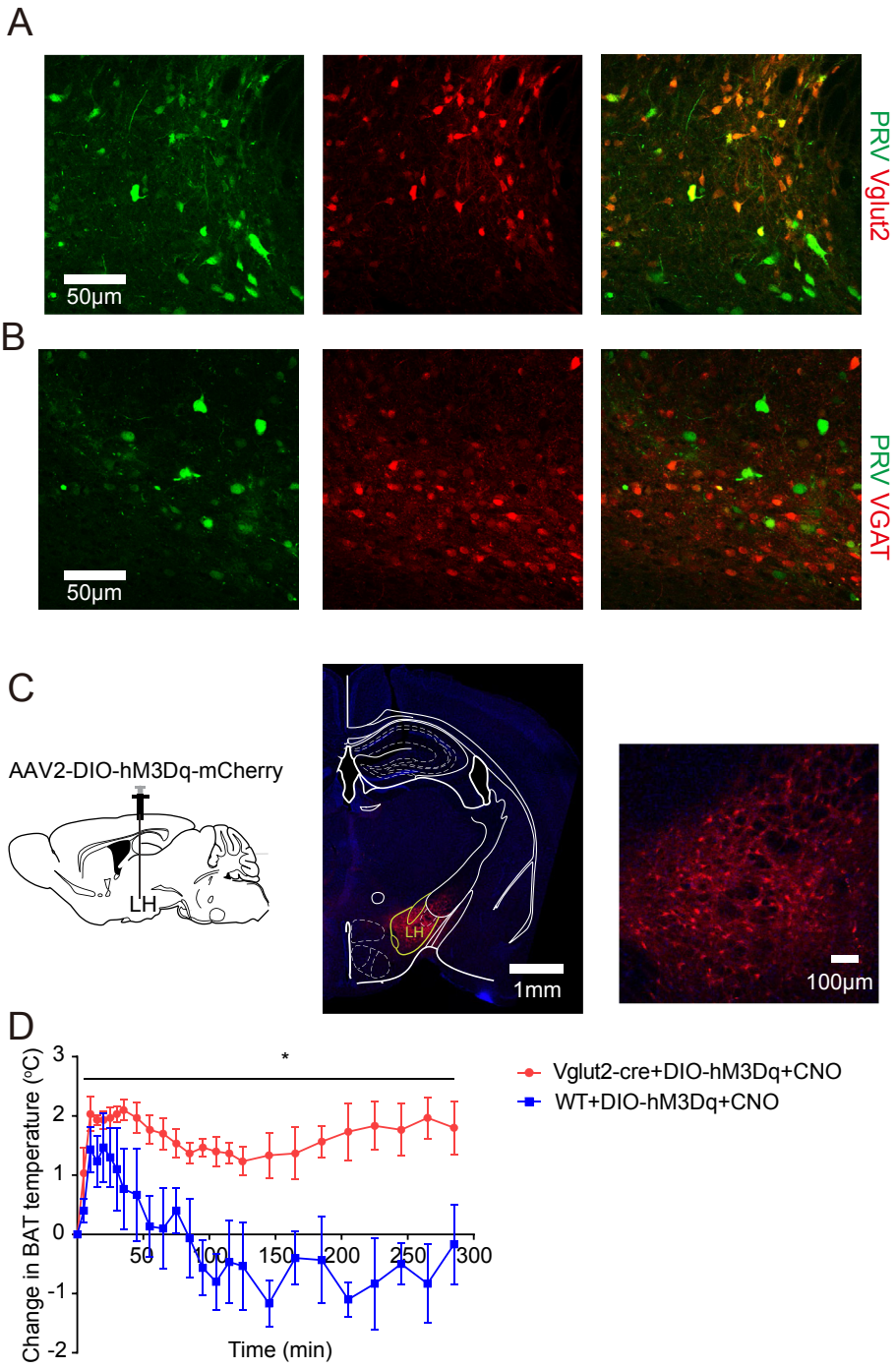

Figure 8: Characterization of BAT-connected neurons in LH. (A—B) Co-localization of VGLUT2-positive glutamatergic neurons, but not VGAT-positive GABAergic neurons, with markers for BAT-connected neurons in LH. Glutamatergic or GABAergic neurons were labeled with Cre-dependent expression of mCherry (red) in the LH of Vglut2-or Vgat-IRES-Cre mice, and BAT-connected neurons were labeled by transsynaptic, retrograde-tracing virus PRV-152-GFP (green). Glutamatergic neurons: VGLUT2+, 64 neurons; PRV+, 50 neurons; VGLUT2+/PRV + double-labeled, 48 neurons; GABAergic neurons: VGAT+, 10 neurons; PRV+, 32 neurons; VGLUT2+/PRV + double-labeled, 1 neuron. **(C)** Chemogenetic stimulation of glutamatergic neurons in LH. Left, schematic diagram of chemogenetic strategy. Cre-dependent AAV expressing excitatory DREADD receptor (hM3Dq) was injected into the LH of Vglut2-IRES-Cre or WT mice. As such, all Vglut2-positive neurons express DREADD. Middle, injection site of AAV-DIO-hM3Dq-mCherry. Right, enlargement of the infected LH region. **(D)** Change in BAT temperatures after intraperitoneal injection of hM3Dq ligand CNO (1 mg/kg) in both Vglut2-IRES-Cre (n = 3) and WT (n = 3) mice. BAT temperatures were recorded by a micro-thermosensor (IPTT-300). Note that intraperitoneal injection—induced stress would lead to a transient increase in BAT temperature in all mice, and the Vglut group showed a sustained elevation of BAT temperatures for more than 4 h. Two-way repeated-measures analysis of variance, $F(1, 4) = 10.77$, $P = 0.0305$.

a >90% overlap between the PRV-GFP and mCherry—positive cells (data not shown), suggesting that most BAT-connected neurons are glutamatergic.

Orexin [42] and melanin concentrating hormone (MCH) [43—45] are two neuropeptides known for their roles in energy expenditure. We next determined their relationships with the *Bdnf*-e1—expressing BAT-

connected neurons in LH. Immunostaining was performed on brain sections derived from the PRV-infected mice, using anti-orexin or anti-MCH antibody. Many neurons were stained positively for orexin (Figure S6A) or MCH (Figure S6B). However, there was minimal overlap between the BAT-connected neurons and the orexin- or MCH-positive neurons. Quantitative analyses revealed there were only 9.46 ± 1.97% orexin-positive neurons among all BAT-connected neurons. Moreover, there were only 12.69 ± 3.95% BAT-connected neurons among all orexin-positive neurons. Similarly, 9.58 ± 1.88% BAT-connected neurons were MCH positive, and 19.21 ± 2.95% MCH-positive neurons were BAT connected (mean ± SEM, n = 3 mice). Thus, most BAT-connected (or thermogenesis-related) neurons in LH expressed *Bdnf* promoter I (*Bdnf-e1*+) but not orexin or MCH. Finally, to determine whether these neurons could regulate thermogenesis directly, we activated LH glutamatergic neurons by chemogenetics combined with BAT temperature recording. Designed human M3 muscarinic receptor coupled to Gq (hM3Dq) was expressed in glutamatergic neurons by injecting a Cre-dependent hM3Dq-mCherry virus in the LH of Vglut2-IRES-Cre mice (Figure 8C). We next implanted micro-thermosensors (IPTT-300) subcutaneously above the BAT to record the BAT temperature (see the Methods section). After intraperitoneal injection of clozapine-N-oxide (CNO; 1 mg/kg), which could bind hM3Dq to activate neurons, we measured the BAT temperature of both Vglut2-IRES-Cre and WT mice over time. We found that the BAT temperature increased about 6% and was sustained over 4 h after providing CNO in Vglut2-IRES-cre mice, while in WT mice, the BAT temperature also increased transiently but went back to the normal state less than 1 h after CNO injection (Figure 8D). Given that *Bdnf-e1*+/BAT-connected neurons are glutamatergic, the chemogenetics experiments provide further support that the BAT-connected glutamatergic neurons in LH play an important role in thermogenesis regulation.

4. DISCUSSION

The present study began by addressing the role of specific *Bdnf* promoters in obesity and thermogenesis. Unexpectedly, we found a specific subpopulation of glutamatergic neurons in the LH that plays a key role in thermogenesis.

An important discovery of the present study is the identification of a new hypothalamic region, LH, that mediates BDNF regulation of thermogenesis. Previous studies have found that PVH is also a crucial region for BDNF-enhanced thermogenesis [12]. As we could observe fewer neurons with fainter *Bdnf*-e1—driven eGFP signals in PVH (Figure 4F), the regulation of BDNF-enhanced thermogenesis by PVH should rely on other BDNF promoters. Thus, we examined *Bdnf*-e4 and *Bdnf*-e6 expression in *Bdnf*-e4 and -e6$^{-/-}$ mice respectively, and found moderate GFP expression in the PVH region (Fig. S7), suggesting a potential role of *Bdnf*-e4 and/or *Bdnf*-e6 in the PVH-mediated regulation of energy balance. However, we found normal BAT morphology and no expression change of thermogenic genes in *Bdnf-e4* (Figure 2) and -e6$^{-/-}$ mice (Figure S8). Thus, promoters other than e1, e4, and e6 may also participate in the PVH regulation of thermogenesis. Future studies will be necessary to clarify these issues. Moreover, other brain regions involved in BDNF regulation of thermogenesis remain to be identified.

LH contains multiple neuronal types that are involved in a plethora of functions, including sleep-wake regulation [46—48], reward seeking [49—51], feeding [51—56], glucose homeostasis [43], and stress responses [57]. Although a pharmacological study has shown that administration of NMDA or bicuculline (a GABA antagonist) to rat LH increased BAT temperature as well as sympathetic nerve activity [30], it is unclear what types of neurons in LH are involved and how they elicit thermogenesis regulation. Using the PRV transsynaptic, retrograde tracing method [37], we labeled all neurons functionally connected to BAT and therefore presumably the neural circuits controlling BAT-mediated thermogenesis. In conjunction with *Bdnf*-e1—eGFP immunostaining, we found that only a subset of BAT-connected neurons in the brain co-expressed *Bdnf*-e1 transcript, and these neurons were virtually all localized in LH. These results imply that thermogenesis regulation may be achieved by *Bdnf*-e1—mediated BDNF expression in the BAT-connected neurons in LH. To determine the type(s) and characteristics of *Bdnf-e1*+/BAT-connected neurons in LH, we have performed double-staining of the BAT-connected neurons and several candidate transmitters/neuropeptides previously implicated in energy balance. Orexin and MCH, two abundant neuropeptides in LH, have been implicated in energy homeostasis [4,43—45,58—62]. Administration of orexin to rRPa, an orexin receptor expressing nucleus known to be involved in thermogenesis, has been shown to enhance sympathetic nerve activity in BAT [30,63]. Thus, the LH orexin neurons projecting to rRPa could regulate thermogenesis by releasing orexin in this target region. Interestingly, ablation of orexin-expressing neurons, but not deletion of the orexin gene, altered cold defensive thermogenesis in mice [64], implying that factors other than orexin in the orexin-expressing neurons may contribute to adaptive thermogenesis regulation [65]. Our study showed that the BAT-connected, *Bdnf*-e1—expressing neurons in LH are not orexin positive, suggesting that BDNF expression through *Bdnf* promoter I may be a new player in addition to, or complementary with, orexin-expressing neurons in LH, for thermogenesis regulation. As for MCH, most previous studies have focused on its roles in food intake [44] and insulin resistance [62], rather than thermogenesis. Our study here found that very few BAT-connected neurons in LH expressed MCH, making them less likely to be involved in BAT-related thermogenesis directly. Most importantly, our experiments revealed that these BAT-connected neurons were Vglut2+ excitatory neurons, but not GABAergic inhibitory neurons. Perhaps, orexin (or MCH) neurons interact with the *Bdnf*-e1—expressing glutamatergic neurons locally in LH to modulate thermogenesis indirectly.

Another interesting observation we made was that the *Bdnf*-e1—expressing neurons in LH also expressed its receptor, TrkB. To determine whether activation of TrkB in these neurons locally could modulate their own neural plasticity by BDNF-TrkB signaling, we delivered a TrkB agonistic antibody locally to LH of *Bdnf*-e1$^{-/-}$ mice. Indeed, infusion of the TrkB-agomab to LH successfully rescued their thermogenesis deficits, including the decrease in thermogenic genes *Ucp1* and the impairment in body response to cold (Figure 7F,G) in *Bdnf*-e1$^{-/-}$ mice. While this result is interesting, there are a number of concerns. First, we have shown that the application of TrkB-agomab could trigger the downstream signaling pathways, PLC-γ, AKT, and MAPK, by western blot analysis in primary cultured hypothalamic neurons. Because of the lack of phospho-PLC-γ, -AKT, and -MAPK antibodies for reliable immunostaining, it is difficult to detect those signaling pathways in TrkB + neurons of LH *in vivo*. Using c-Fos immunostaining to reveal TrkB-agomab—induced neuronal activation, we now show that c-Fos was induced in TrkB + neurons 2 h after the infusion of TrkB-agomab in LH (Figure S9A), while only a few c-Fos + neurons were detected after the administration of control IgG (Figure S9B). These data suggest that TrkB-agomab could also activate neurons *in vivo*. Second, given that TrkB is widely expressed in regions outside LH, we need to address whether TrkB agonist antibody also activated neurons outside LH. We found that TrkB-agomab was confined to the LH region 2 weeks after microinjection (Figure 7E).

While a minute amount of TrkB-agomab could still diffuse outside LH, it was beyond the detection limit of TrkB staining (Figure 7E), and its concentration may not be high enough to activate TrkB. Third, TrkB-agomab injected into LH could act on TrkB-expressing afferent axons from another brain-innervating LH. Our current data cannot rule out this possibility. Fourth, although TrkB-agomab could rescue thermogenesis deficits, direct infusion of TrkB-agomab in such a small brain region of the hypothalamus could not completely overturn the obesity phenotype in *Bdnf*-e1$^{-/-}$ mice (data not shown). These results suggest that *Bdnf*-e1 expression in BAT-connected neurons in LH are necessary, but not sufficient, for thermogenesis regulation. Perhaps some other brain regions also participate in thermogenesis through *Bdnf*-e1—derived BDNF expression. Future studies will be necessary to clarify these issues.

One may also ask why recombinant BDNF protein or BDNF-expressing virus are not used instead of TrkB-agomab. The advantages of using TrkB-agomab are its long half-life as well as its specificity on the TrkB and not p75^{NTR}. TrkB-agomab injected into the brain could last for days or even more than a week (Wei et al., submitted). Thus, a single injection of the antibody into LH resulted in an increase in *Ucp1* expression for as long as 2 weeks (Figure 7F). In contrast, the t1/2 of BDNF is only a few hours [66], and therefore, BDNF needs to be delivered constantly through a cannula implantation of an osmotic pump. Viral expression of BDNF could avoid the short t1/2 problem, but it may elicit some unwanted side effects caused by overexpression and/or activation of its low-affinity receptor p75^{NTR} in addition to TrkB. We show that activation of the Vglut2+ neurons in LH by chemogenetic tools resulted in a rise in BAT temperature (Figures 8C and 5D), suggesting a causal relationship between LH Vglut2+ neurons and BAT thermogenesis. One may argue that some Vglut2+ neurons were activated that are not BAT connected. However, our preliminary results showed that the Vglut2+ BAT-connected neurons were largely overlapping. To completely alleviate this concern, one would need to activate only BAT-connected neurons but not other excitatory neurons in LH. This is difficult, since the current version of multisynaptic retrograde tracing tools such as PRV is toxic to certain extent. In our observation, mice died within 2 weeks after infection with the virus, whether no matter PRV-614 (red) or −152 (green) was injected into BAT. This prohibited the expression of chemogenetic or optogenetic genes specifically in the BAT-connected neurons. Future work using single-cell transcriptomic analysis should identify the specific markers for BAT-connected neurons and therefore manipulate these LH neurons specifically. To determine whether the deficit of BAT thermogenesis is the cause or the consequence of obesity, we have performed experiments using *Bdnf-e1*$^{-/-}$ mice of 10—11 weeks of age, when body weight just begins to rise. At this age, both the body weight and body length had a trend of increase but showed no significance (Figure 3A,B). However, the BAT weight (Figure 3C) and *Ucp1* (Figure 3D) expression in *Bdnf-e1*$^{-/-}$ mice were significantly decreased compared with those in WT mice. Moreover, we found that the level of TH was also obviously decreased (Figure 3E), indicating a reduced sympathetic outflow well before the overt obesity phenotype was observed. Taken together, while we cannot say that the deficits of BAT thermogenesis were the cause of obesity, they could be important contributors to the obesity phenotype in *Bdnf-e1*$^{-/-}$ mice.

It remains to be determined whether *Bdnf*-e1$^{-/-}$ mice may have other deficits in energy balance in addition to thermogenesis. In a recent study, McAllan et al. reported a hyperphagia phenotype in the same *Bdnf*-e1$^{-/-}$ mice [67]. However, under our experimental conditions, we have not seen an obvious hyperphagia phenotype (Figure S10). Careful comparison of the two studies suggest that the major difference may lie in the housing strategies. Specifically, McAllan et al. housed two animals in a cage with a transparent divider to avoid the aggressive attacks by the *Bdnf-e1*$^{-/-}$ mice mutants, while we group-housed all WT and mutant mice from the same mother to eliminate aggressive behavior. Thus, we hypothesized that early social isolation coupled with *Bdnf*-e1 knockout (environment X gene, "G X E"), but not *Bdnf*-e1 knockout alone, could lead to hyperphagia reported in the McAllan et al. study. Perhaps *Bdnf*-e1 expression in brain regions other than LH may play a role in this "G X E" process, regulating body weight through controlling food intake. Further studies are necessary to understand the other factors that contribute to the obesity phenotype regulated by *Bdnf*-e1 and to test the G X E hypothesis described above.

5. CONCLUSION

In summary, we found that genetic inhibition of *Bdnf* promoter I (*Bdnf*-e1$^{-/-}$), but not promoters IV (*Bdnf*-e4$^{-/-}$) or VI (*Bdnf*-e6$^{-/-}$), resulted in deficits in BAT-mediated thermogenesis. Transsynaptic, retrograde tracing of the BAT-connected neuronal circuit combined with GFP labeling of *Bdnf*-e1—expressing cells demonstrated that in LH, the BAT-connected neurons largely coincide with *Bdnf*-e1 expression. Disruption of *Bdnf*-e1 expression in these neurons impaired body temperature response to cold as well as BAT expression of thermogenesis genes *Ucp1* and *Pcg1a*. Activation of these neurons by either TrkB agonists or chemogenetic tools enhanced BAT-mediated thermogenesis. Taken together, these results have unraveled a unique subset of LH neurons critical for thermogenesis regulation and provide new insights into how different *Bdnf* promoters could control many different brain functions.

AUTHOR CONTRIBUTIONS

H.Y., P.C., W.G., and B.L. initiated the project and designed the study. H.Y. and P.C. conducted the experiments and analyzed the data. B.L., H.Y., and P.C. wrote the manuscript.

ACKNOWLEDGMENT

We thank Drs. Bei Shan and Xiaoming Guan for their suggestions. We are greatly thankful for the technical support of the Metabolomics Facility at the Technology Center for Protein Sciences at Tsinghua University. This work was supported by the National Natural Science Foundation of China (31730034, 81501105), Beijing Municipal Science & Technology Commission (Z151100003915118), and Shenzhen Science, Technology and Innovation Commission (JCYJ20170411152419928 and GJHZ20170314151528005) to B.L.

CONFLICT OF INTEREST

The authors declare no conflict of interests.

APPENDIX A. SUPPLEMENTARY DATA

Supplementary data to this article can be found online at https://doi.org/10.1016/j.molmet.2019.11.013.

REFERENCES

[1] Garland Jr., T., Schutz, H., Chappell, M.A., Keeney, B.K., Meek, T.H., Copes, L.E., et al., 2011. The biological control of voluntary exercise, spontaneous physical activity and daily energy expenditure in relation to obesity:

human and rodent perspectives. Journal of Experimental Biology 214(Pt 2): 206–229.
[2] Abreu-Vieira, G., Xiao, C., Gavrilova, O., Reitman, M.L., 2015. Integration of body temperature into the analysis of energy expenditure in the mouse. Molecular Metabolism 4(6):461–470.
[3] Clapham, J.C., 2012. Central control of thermogenesis. Neuropharmacology 63(1):111–123.
[4] Morrison, S.F., Madden, C.J., Tupone, D., 2014. Central neural regulation of brown adipose tissue thermogenesis and energy expenditure. Cell Metabolism 19(5):741–756.
[5] Cannon, B., Nedergaard, J., 2004. Brown adipose tissue: function and physiological significance. Physiological Reviews 84(1):277–359.
[6] Xu, B., Xie, X., 2016. Neurotrophic factor control of satiety and body weight. Nature Reviews Neuroscience 17(5):282–292.
[7] Morrison, S.F., Madden, C.J., Tupone, D., 2012. Central control of brown adipose tissue thermogenesis. Frontiers in Endocrinology (Lausanne) 3(JAN).
[8] Han, J.C., Liu, Q.R., Jones, M., Levinn, R.L., Menzie, C.M., Jefferson-George, K.S., et al., 2008. Brain-derived neurotrophic factor and obesity in the WAGR syndrome. New England Journal of Medicine 359(9):918–927.
[9] Kernie, S.G., Liebl, D.J., Parada, L.F., 2000. BDNF regulates eating behavior and locomotor activity in mice. The EMBO Journal 19(6):1290–1300.
[10] Lyons, W.E., Mamounas, L.A., Ricaurte, G.A., Coppola, V., Reid, S.W., Bora, S.H., et al., 1999. Brain-derived neurotrophic factor-deficient mice develop aggressiveness and hyperphagia in conjunction with brain serotonergic abnormalities. Proceedings of the National Academy of Sciences of the United States of America 96(26):15239–15244.
[11] Xu, B., Goulding, E.H., Zang, K., Cepoi, D., Cone, R.D., Jones, K.R., et al., 2003. Brain-derived neurotrophic factor regulates energy balance downstream of melanocortin-4 receptor. Nature Neuroscience 6(7):736–742.
[12] An, J.J., Liao, G.Y., Kinney, C.E., Sahibzada, N., Xu, B., 2015. Discrete BDNF neurons in the paraventricular hypothalamus control feeding and energy expenditure. Cell Metabolism 22(1):175–188.
[13] Nonomura, T., Tsuchida, A., Ono-Kishino, M., Nakagawa, T., Taiji, M., Noguchi, H., 2001. Brain-derived neurotrophic factor regulates energy expenditure through the central nervous system in obese diabetic mice. International Journal of Experimental Diabetes Research 2(3):201–209.
[14] Wang, C., Bomberg, E., Billington, C.J., Levine, A.S., Kotz, C.M., 2010. Brain-derived neurotrophic factor (BDNF) in the hypothalamic ventromedial nucleus increases energy expenditure. Brain Research 1336:66–77.
[15] Wang, C., Bomberg, E., Billington, C., Levine, A., Kotz, C.M., 2007. Brain-derived neurotrophic factor in the hypothalamic paraventricular nucleus increases energy expenditure by elevating metabolic rate. American Journal of Physiology - Regulatory, Integrative and Comparative Physiology 293(3): R992–R1002.
[16] Barde, Y.A., 1994. Neurotrophins: a family of proteins supporting the survival of neurons. Progress in Clinical and Biological Research 390:45–56.
[17] Ceni, C., Unsain, N., Zeinieh, M.P., Barker, P.A., 2014. Neurotrophins in the regulation of cellular survival and death. Handbook of Experimental Pharmacology 220:193–221.
[18] Greenberg, M.E., Xu, B., Lu, B., Hempstead, B.L., 2009. New insights in the biology of BDNF synthesis and release: implications in CNS function. Journal of Neuroscience 29(41):12764–12767.
[19] Kaplan, D.R., Miller, F.D., 2007. Developing with BDNF: a moving experience. Neuron 55(1):1–2.
[20] Lu, B., 2003. BDNF and activity-dependent synaptic modulation. Learning & Memory 10(2):86–98.
[21] Lu, B., Nagappan, G., Guan, X., Nathan, P.J., Wren, P., 2013. BDNF-based synaptic repair as a disease-modifying strategy for neurodegenerative diseases. Nature Reviews Neuroscience 14(6):401–416.
[22] Timmusk, T., Palm, K., Metsis, M., Reintam, T., Paalme, V., Saarma, M., et al., 1993. Multiple promoters direct tissue-specific expression of the rat BDNF gene. Neuron 10(3):475–489.
[23] Martinowich, K., Manji, H., Lu, B., 2007. New insights into BDNF function in depression and anxiety. Nature Neuroscience 10(9):1089–1093.
[24] Jiao, Y., Zhang, Z., Zhang, C., Wang, X., Sakata, K., Lu, B., et al., 2011. A key mechanism underlying sensory experience-dependent maturation of neocortical GABAergic circuits in vivo. Proceedings of the National Academy of Sciences of the United States of America 108(29):12131–12136.
[25] Martinowich, K., Schloesser, R.J., Jimenez, D.V., Weinberger, D.R., Lu, B., 2011. Activity-dependent brain-derived neurotrophic factor expression regulates cortistatin-interneurons and sleep behavior. Molecular Brain 4(1).
[26] Sakata, K., Martinowich, K., Woo, N.H., Schloesser, R.J., Jimenez, D.V., Ji, Y., et al., 2013. Role of activity-dependent BDNF expression in hippocampal-prefrontal cortical regulation of behavioral perseverance. Proceedings of the National Academy of Sciences of the United States of America 110(37): 15103–15108.
[27] Sakata, K., Woo, N.H., Martinowich, K., Greene, J.S., Schloesser, R.J., Shen, L., et al., 2009. Critical role of promoter IV-driven BDNF transcription in GABAergic transmission and synaptic plasticity in the prefrontal cortex. Proceedings of the National Academy of Sciences of the United States of America 106(14):5942–5947.
[28] Maynard, K.R., Hill, J.L., Calcaterra, N.E., Palko, M.E., Kardian, A., Paredes, D., et al., 2016. Functional role of BDNF production from unique promoters in aggression and serotonin signaling. Neuropsychopharmacology 41(8):1943–1955.
[29] Chouchani, E.T., Kazak, L., Jedrychowski, M.P., Lu, G.Z., Erickson, B.K., Szpyt, J., et al., 2016. Mitochondrial ROS regulate thermogenic energy expenditure and sulfenylation of UCP1. Nature 532(7597):112–116.
[30] Tupone, D., Madden, C.J., Cano, G., Morrison, S.F., 2011. An orexinergic projection from perifornical hypothalamus to raphe pallidus increases rat brown adipose tissue thermogenesis. Journal of Neuroscience 31(44):15944–15955.
[31] Changou, C.A., Ajoy, R., Chou, S.Y., 2017. Live images of GLUT4 protein trafficking in mouse primary hypothalamic neurons using deconvolution microscopy. Journal of Visualized Experiments(130).
[32] Pruunsild, P., Sepp, M., Orav, E., Koppel, I., Timmusk, T., 2011. Identification of cis-elements and transcription factors regulating neuronal activity-dependent transcription of human BDNF gene. Journal of Neuroscience 31(9):3295–3308.
[33] Shi, B., Xie, S., Berryman, D., List, E., Liu, J., 2013. Robust separation of visceral and subcutaneous adipose tissues in micro-CT of mice. Conference Proceeding of IEEE Engineering in Medicine and Biology Society 2013:2312–2315.
[34] Morrison, S.F., 2016. Central neural control of thermoregulation and brown adipose tissue. Autonomic Neuroscience Basic and Clinical 196:14–24.
[35] Cerri, M., Morrison, S.F., 2005. Activation of lateral hypothalamic neurons stimulates brown adipose tissue thermogenesis. Neuroscience 135(2):627–638.
[36] Bamshad, M., Song, C.K., Bartness, T.J., 1999. CNS origins of the sympathetic nervous system outflow to brown adipose tissue. American Journal of Physiology 276(6 Pt 2):R1569–R1578.
[37] Oldfield, B.J., Giles, M.E., Watson, A., Anderson, C., Colvill, L.M., McKinley, M.J., 2002. The neurochemical characterisation of hypothalamic pathways projecting polysynaptically to brown adipose tissue in the rat. Neuroscience 110(3):515–526.
[38] Ryu, V., Garretson, J.T., Liu, Y., Vaughan, C.H., Bartness, T.J., 2015. Brown adipose tissue has sympathetic-sensory feedback circuits. Journal of Neuroscience 35(5):2181–2190.
[39] Ji, Y., Lu, Y., Yang, F., Shen, W., Tang, T.T., Feng, L., et al., 2010. Acute and gradual increases in BDNF concentration elicit distinct signaling and functions in neurons. Nature Neuroscience 13(3):302–309.

[40] Han, F., Guan, X., Guo, W., Lu, B., 2019. Therapeutic potential of a TrkB agonistic antibody for ischemic brain injury. Neurobiology of Disease 127:570–581.
[41] Chen, M., Chen, H., Nguyen, A., Gupta, D., Wang, J., Lai, E.W., et al., 2010. G(s)alpha deficiency in adipose tissue leads to a lean phenotype with divergent effects on cold tolerance and diet-induced thermogenesis. Cell Metabolism 11(4):320–330.
[42] Hara, J., Beuckmann, C.T., Nambu, T., Willie, J.T., Chemelli, R.M., Sinton, C.M., et al., 2001. Genetic ablation of orexin neurons in mice results in narcolepsy, hypophagia, and obesity. Neuron 30(2):345–354.
[43] Kong, D., Vong, L., Parton, L.E., Ye, C., Tong, Q., Hu, X., et al., 2010. Glucose stimulation of hypothalamic MCH neurons involves K(ATP) channels, is modulated by UCP2, and regulates peripheral glucose homeostasis. Cell Metabolism 12(5):545–552.
[44] Qu, D., Ludwig, D.S., Gammeltoft, S., Piper, M., Pelleymounter, M.A., Cullen, M.J., et al., 1996. A role for melanin-concentrating hormone in the central regulation of feeding behaviour. Nature 380(6571):243–247.
[45] Shimada, M., Tritos, N.A., Lowell, B.B., Flier, J.S., Maratos-Flier, E., 1998. Mice lacking melanin-concentrating hormone are hypophagic and lean. Nature 396(6712):670–679.
[46] Adamantidis, A.R., Zhang, F., Aravanis, A.M., Deisseroth, K., de Lecea, L., 2007. Neural substrates of awakening probed with optogenetic control of hypocretin neurons. Nature 450(7168):420–424.
[47] Liu, K., Kim, J., Kim, D.W., Zhang, Y.S., Bao, H., Denaxa, M., et al., 2017. Lhx6-positive GABA-releasing neurons of the zona incerta promote sleep. Nature 548(7669):582–587.
[48] Naganuma, F., Kroeger, D., Bandaru, S.S., Absi, G., Madara, J.C., Vetrivelan, R., 2019. Lateral hypothalamic neurotensin neurons promote arousal and hyperthermia. PLoS Biology 17(3):e3000172.
[49] Harris, G.C., Wimmer, M., Aston-Jones, G., 2005. A role for lateral hypothalamic orexin neurons in reward seeking. Nature 437(7058):556–559.
[50] Nieh, E.H., Vander Weele, C.M., Matthews, G.A., Presbrey, K.N., Wichmann, R., Leppla, C.A., et al., 2016. Inhibitory input from the lateral hypothalamus to the ventral tegmental area disinhibits dopamine neurons and promotes behavioral activation. Neuron 90(6):1286–1298.
[51] Stuber, G.D., Wise, R.A., 2016. Lateral hypothalamic circuits for feeding and reward. Nature Neuroscience 19(2):198–205.
[52] Sakurai, T., Amemiya, A., Ishii, M., Matsuzaki, I., Chemelli, R.M., Tanaka, H., et al., 1998. Orexins and orexin receptors: a family of hypothalamic neuropeptides and G protein-coupled receptors that regulate feeding behavior. Cell 92(4):573–585.
[53] Leinninger, G.M., Jo, Y.H., Leshan, R.L., Louis, G.W., Yang, H., Barrera, J.G., et al., 2009. Leptin acts via leptin receptor-expressing lateral hypothalamic neurons to modulate the mesolimbic dopamine system and suppress feeding. Cell Metabolism 10(2):89–98.
[54] Jennings, J.H., Rizzi, G., Stamatakis, A.M., Ung, R.L., Stuber, G.D., 2013. The inhibitory circuit architecture of the lateral hypothalamus orchestrates feeding. Science 341(6153):1517–1521.
[55] O'Connor, E.C., Kremer, Y., Lefort, S., Harada, M., Pascoli, V., Rohner, C., et al., 2015. Accumbal D1R neurons projecting to lateral hypothalamus authorize feeding. Neuron 88(3):553–564.
[56] Lopez-Ferreras, L., Richard, J.E., Noble, E.E., Eerola, K., Anderberg, R.H., Olandersson, K., et al., 2018. Lateral hypothalamic GLP-1 receptors are critical for the control of food reinforcement, ingestive behavior and body weight. Molecular Psychiatry 23(5):1157–1168.
[57] Bonnavion, P., Jackson, A.C., Carter, M.E., de Lecea, L., 2015. Antagonistic interplay between hypocretin and leptin in the lateral hypothalamus regulates stress responses. Nature Communications 6:6266.
[58] Baird, J.P., Choe, A., Loveland, J.L., Beck, J., Mahoney, C.E., Lord, J.S., et al., 2009. Orexin-A hyperphagia: hindbrain participation in consummatory feeding responses. Endocrinology 150(3):1202–1216.
[59] Blouin, A.M., Fried, I., Wilson, C.L., Staba, R.J., Behnke, E.J., Lam, H.A., et al., 2013. Human hypocretin and melanin-concentrating hormone levels are linked to emotion and social interaction. Nature Communications 4:1547.
[60] Hausen, A.C., Ruud, J., Jiang, H., Hess, S., Varbanov, H., Kloppenburg, P., et al., 2016. Insulin-dependent activation of MCH neurons impairs locomotor activity and insulin sensitivity in obesity. Cell Reports 17(10):2512–2521.
[61] Ito, M., Gomori, A., Ishihara, A., Oda, Z., Mashiko, S., Matsushita, H., et al., 2003. Characterization of MCH-mediated obesity in mice. American Journal of Physiology. Endocrinology and Metabolism 284(5):E940–E945.
[62] Ludwig, D.S., Tritos, N.A., Mastaitis, J.W., Kulkarni, R., Kokkotou, E., Elmquist, J., et al., 2001. Melanin-concentrating hormone overexpression in transgenic mice leads to obesity and insulin resistance. Journal of Clinical Investigation 107(3):379–386.
[63] Berthoud, H.R., Patterson, L.M., Sutton, G.M., Morrison, C., Zheng, H., 2005. Orexin inputs to caudal raphe neurons involved in thermal, cardiovascular, and gastrointestinal regulation. Histochemistry and Cell Biology 123(2):147–156.
[64] Takahashi, Y., Zhang, W., Sameshima, K., Kuroki, C., Matsumoto, A., Sunanaga, J., et al., 2013. Orexin neurons are indispensable for prostaglandin E2-induced fever and defence against environmental cooling in mice. Journal of Physiology 591(22):5623–5643.
[65] Zhang, W., Sunanaga, J., Takahashi, Y., Mori, T., Sakurai, T., Kanmura, Y., et al., 2010. Orexin neurons are indispensable for stress-induced thermogenesis in mice. Journal of Physiology 588(Pt 21):4117–4129.
[66] Dittrich, F., Ochs, G., Grosse-Wilde, A., Berweiler, U., Yan, Q., Miller, J.A., et al., 1996. Pharmacokinetics of intrathecally applied BDNF and effects on spinal motoneurons. Experimental Neurology 141(2):225–239.
[67] McAllan, L., Maynard, K.R., Kardian, A.S., Stayton, A.S., Fox, S.L., Stephenson, E.J., et al., 2018. Disruption of brain-derived neurotrophic factor production from individual promoters generates distinct body composition phenotypes in mice. American Journal of Physiology Endocrinology and Metabolism 315(6):1168–e1184.

